Neuronal calcium-binding proteins 1/2 localize to dorsal root ganglia and excitatory spinal neurons and are regulated by nerve injury

Ming-Dong Zhang[a,b,1], Giuseppe Tortoriello[b], Brian Hsueh[c,d], Raju Tomer[c,d], Li Ye[c,d], Nicholas Mitsios[e], Lotta Borgius[a], Gunnar Grant[a], Ole Kiehn[a], Masahiko Watanabe[f], Mathias Uhlén[g], Jan Mulder[a,e], Karl Deisseroth[c,d], Tibor Harkany[b,h,2], and Tomas G. M. Hökfelt[a,1,2]

[a]Department of Neuroscience, [b]Division of Molecular Neurobiology, Department of Medical Biochemistry and Biophysics, and [e]Science for Life Laboratory, Department of Neuroscience, Karolinska Institutet, 17177 Stockholm, Sweden; [c]Departments of Bioengineering and Psychiatry and [d]Howard Hughes Medical Institute, Stanford University, Stanford, CA 94305; [f]Hokkaido University School of Medicine, Sapporo 060-8638, Japan; [g]Science for Life Laboratory, Albanova University Center, Royal Institute of Technology, 10691 Stockholm, Sweden; and [h]Department of Molecular Neurosciences, Center for Brain Research, Medical University of Vienna, A-1090 Vienna, Austria

Contributed by Tomas G. M. Hökfelt, February 6, 2014 (sent for review January 17, 2014)

Neuronal calcium (Ca^{2+})-binding proteins 1 and 2 (NECAB1/2) are members of the phylogenetically conserved EF-hand Ca^{2+}-binding protein superfamily. To date, NECABs have been explored only to a limited extent and, so far, not at all at the spinal level. Here, we describe the distribution, phenotype, and nerve injury-induced regulation of NECAB1/NECAB2 in mouse dorsal root ganglia (DRGs) and spinal cord. In DRGs, NECAB1/2 are expressed in around 70% of mainly small- and medium-sized neurons. Many colocalize with calcitonin gene-related peptide and isolectin B4, and thus represent nociceptors. NECAB1/2 neurons are much more abundant in DRGs than the Ca^{2+}-binding proteins (parvalbumin, calbindin, calretinin, and secretagogin) studied to date. In the spinal cord, the NECAB1/2 distribution is mainly complementary. NECAB1 labels interneurons and a plexus of processes in superficial layers of the dorsal horn, commissural neurons in the intermediate area, and motor neurons in the ventral horn. Using CLARITY, a novel, bilaterally connected neuronal system with dendrites that embrace the dorsal columns like palisades is observed. NECAB2 is present in cell bodies and presynaptic boutons across the spinal cord. In the dorsal horn, most NECAB1/2 neurons are glutamatergic. Both NECAB1/2 are transported into dorsal roots and peripheral nerves. Peripheral nerve injury reduces NECAB2, but not NECAB1, expression in DRG neurons. Our study identifies NECAB1/2 as abundant Ca^{2+}-binding proteins in pain-related DRG neurons and a variety of spinal systems, providing molecular markers for known and unknown neuron populations of mechanosensory and pain circuits in the spinal cord.

commissural interneurons | GAD67 | neuropathic pain | VGLUT2

Calcium (Ca^{2+}) plays a crucial role in many and diverse cellular processes, including neurotransmission (1). Glutamate and neuropeptides are neurotransmitters released from the central terminals of dorsal root ganglion (DRG) neurons in the spinal dorsal horn, where signals for different sensory modalities, including pain, are conveyed to higher centers (2–12). Neurotransmitter release is tightly regulated by Ca^{2+}-dependent SNARE proteins whose activity is regulated by Ca^{2+}-binding proteins (CaBPs) (1, 7, 13).

Parvalbumin (PV), calbindin D-28K (CB), calretinin (CR), and secretagogin (Scgn) are extensively studied EF-hand CaBPs, and they have also emerged as valuable anatomical markers for morphologically and functionally distinct neuronal subpopulations (14–17). The expression of CaBPs in DRG neurons has been thoroughly studied (18). Moreover, neuronal Ca^{2+} sensor 1 and downstream regulatory element-antagonist modulator (DREAM) are also EF-hand Ca^{2+}-binding proteins in DRGs and the spinal cord (19, 20). Despite these advances, a CaBP has so far not been characterized in the majority of small- and medium-sized DRG neurons, many of which represent nociceptors.

The subfamily of neuronal Ca^{2+}-binding proteins (NECABs) consists of three members (NECAB1–NECAB3), probably as a result of gene duplication (21). NECABs are also EF-hand proteins, with one pair of EF-hand motifs in the N terminus and a putative antibiotic biosynthesis monooxygenase domain in the C terminus, which are linked by a NECAB homogeneous region (22). NECAB1/2 are restricted to the nervous system, whereas NECAB3 is also expressed in the heart and skeletal muscle (21).

NECAB1 was first identified as the target protein of synaptotagmin I C2A-domain by affinity chromatography, with its expression restricted to layer 4 cortical pyramidal neurons, inhibitory interneurons, and hippocampal CA2 pyramidal cells in mouse brain (21, 23). The gene of the second member was cloned from mouse and initially named *Necab*. It encodes a 389-aa (NECAB2) (24). NECAB2 was identified as a downstream target of Pax6 in mouse retina, which is involved in retinal development (24, 25), as well as being a binding partner for the adenosine A_{2A} receptor (22). Furthermore, an interaction between NECAB2 and metabotropic glutamate receptor 5 (mGluR5) was demonstrated in rat hippocampal pyramidal cells, possibly regulating mGluR5's coupling to its signaling machinery (26).

Significance

Calcium-binding proteins (CaBPs) are key determinants of cellular functions, as well as useful anatomical markers for neural subpopulations. Here, we reveal the distribution and phenotypes of neurons expressing neuronal calcium-binding proteins 1 and 2 (NECAB1/2) in intact mouse dorsal root ganglia (DRGs) and spinal cord and after nerve injury using immunohistochemistry and the CLARITY method. In DRGs, NECAB1/2 are expressed in high numbers (~70%) of all DRG neurons, including nociceptors. Axonal injury down-regulates NECAB2 in DRGs. In spinal cord, NECAB1/2 show a complementary distribution, mostly in excitatory neurons, and represent unique molecular markers for commissural neurons originally described by Ramón y Cajal. Our characterization of NECABs at the spinal level provides a basis for exploring their role in sensory functions, particularly pain.

Author contributions: M.-D.Z., T.H., and T.G.M.H. designed research; M.-D.Z., G.T., B.H., R.T., L.Y., L.B., and O.K. performed research; N.M., O.K., M.W., M.U., and J.M. contributed new reagents/analytic tools; M.-D.Z., G.G., O.K., J.M., T.H., and T.G.M.H. analyzed data; and M.-D.Z., K.D., T.H., and T.G.M.H. wrote the paper.

The authors declare no conflict of interest.

[1]To whom correspondence may be addressed. E-mail: mingdong.zhang@ki.se or tomas.hokfelt@ki.se.

[2]T.H. and T.G.M.H. contributed equally to this work.

This article contains supporting information online at www.pnas.org/lookup/suppl/doi:10.1073/pnas.1402318111/-/DCSupplemental.

Finally, NECAB3, also known as XB51, was isolated as an interacting target for the neuron-specific X11-like protein and is possibly involved in the pathogenesis of Alzheimer's disease (27, 28).

Very recently, NECAB1/2 were shown to have complementary expression patterns in mouse hippocampus at the mRNA and protein levels, whereas NECAB3 is broadly distributed in the hippocampus (29). NECAB1-expressing cells were seen throughout the cell-sparse layers of Ammon's horn and the hilus of the dentate gyrus. In contrast, NECAB2 is enriched in pyramidal cells of the CA2 region. A minority of NECAB1$^+$ neurons were GABAergic yet did not coexpress PV, CB, or CR (29).

Here, we investigated the expression of NECAB1/2 in mouse DRGs and spinal cord using quantitative PCR (qPCR), immunohistochemistry (also combined with CLARITY) (30), and Western blotting. We compared the distribution of NECABs with that of the four CaBPs restricted to neurons, PV, CB, CR, or Scgn. NECAB$^+$ neurons in the spinal dorsal horn were phenotyped using transgenic mice harboring genetic markers for excitatory [vesicular glutamate transporter 2 (VGLUT2)] (31) or inhibitory [glutamate decarboxylase 67 (GAD67)] (32) cell identities. Finally, the effect of peripheral nerve injury was analyzed.

Results

NECAB1/2 Are Expressed in Pain-Related DRG Neurons. The NECAB1/2 antibodies were validated by Western blotting and antigen adsorption (Fig. S1 *A* and *C*). The anti-NECAB1 antibody revealed a strong band at the calculated molecular mass of the target protein (41 kDa), whereas the NECAB2 antiserum produced two bands at 44 kDa and 39 kDa in protein lysates from mouse DRGs. Previous studies have shown that NECAB2 has two isoforms (43.4 kDa and 39.4 kDa), reflecting two conserved Kozak consensus sequences (Fig. S1*B*; conserved positions are labeled with numbers). Moreover, antibody staining with both NECABs disappeared in adjacent sections upon preincubation with the corresponding antigen at a concentration of 10^{-6} M overnight (Fig. S1*C*). Taken together, these results support specificity for the staining patterns obtained with both NECAB1/2 antisera.

Both NECAB1/2 were abundant in the mouse DRGs and found in 64.9 ± 2.0% and 73.2 ± 1.7% of all propidium iodide-stained neuron profiles (NPs), respectively (Fig. 1*C*). NECAB1 represented cytoplasmic staining of graded intensity, mainly in small- and medium-sized neurons (Fig. 1 *A* and *C*). Intraganglionic axons could also be seen (Fig. 1*C* and Fig. S1*C*). NECAB2 showed a similar staining pattern (Fig. 1 *A* and *C*). The overlapping size distributions, together with the high percentages of total DRG neurons expressing either protein, predict a fairly high degree of coexistence of the two NECABs.

To determine the phenotype of neurons that express NECAB1 or NECAB2, we used the classic peptidergic marker calcitonin gene-related peptide (CGRP); the nonpeptidergic marker isolectin B4 (IB4) from *Griffonia simplicifolia*; and neurofilament 200, a marker for neurons with myelinated axons (Fig. 1 *B* and *C*). NECAB1/2 revealed similar neuronal phenotypes with regard to these markers. Thus, around 40% of the NECAB1$^+$ and NECAB2$^+$ NPs were peptidergic and 25–30% were myelinated (Fig. 1 *B* and *C*). However, 42.5 ± 2.5% of the NECAB1$^+$ neurons colocalized with IB4 vs. only 25.3 ± 2.0% for NECAB2 (Fig. 1 *B* and *C*).

In contrast to the high proportion of NECABs in small- and medium-sized neurons, the three principal CaBPs and Scgn exist in more circumscribed DRG neuron populations, and mainly in small- or large-sized ones (33). In DRGs, 1.1 ± 0.2% of the NECAB1$^+$ NPs were PV$^+$, 9.7 ± 0.8% were CB$^+$, 0.2 ± 0.1% were CR$^+$, and 3.0 ± 1.2% were Scgn$^+$. The corresponding ratios for NECAB2 were 5.8 ± 1.2%, 10.9 ± 1.2%, 0.6 ± 0.2%, and 1.8 ± 0.2%, respectively (Fig. 1*B*). Conversely, many CB$^+$ NPs showed a prominent colocalization with NECAB1 (62.7 ± 12.2%) vs. 11.9 ± 1.9% for PV, 19.9 ± 14.1% for CR, and 49.5 ± 6.1% for Scgn. The same was observed for NECAB2$^+$ neurons (PV: 42.5 ± 9.7%, CB: 72.2 ± 9.8%, CR: 29.3 ± 22.2%, and Scgn: 41.4 ± 5.2%; Fig. 1*D*). Taken together, NECABs represent unique members of CaBPs expressed in a large proportion of the DRG neurons, particularly in those associated with pain signaling.

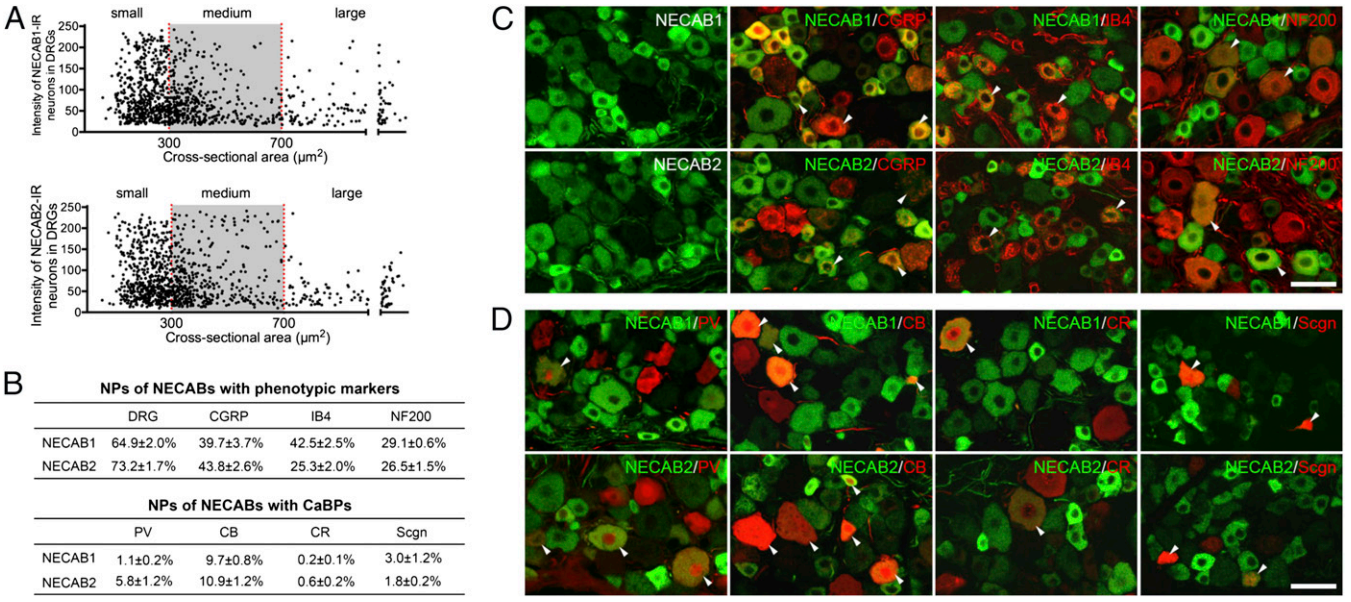

Fig. 1. Expression of NECAB1/2 and colocalization with "classic" markers in lumbar DRGs. (*A*) Fluorescence intensity plotted vs. cross-sectional area of NECAB1/2$^+$ neurons. (*B*) Percentage colocalization of NECABs with CGRP, IB4, or neurofilament 200 (NF200), as well as with "classic" CaBPs. (*C*) Confocal images show colocalization of NECAB1/2$^+$ neurons with CGRP, IB4, or NF200. Arrowheads indicate colocalization (note different intensities). (*D*) Confocal images show colocalization of NECAB1/2$^+$ neurons with PV, CB, CR, or Scgn (arrowheads show examples). (Scale bars: *C* and *D*, 50 μm.)

NECAB1/2 Expression in the Spinal Cord. The expression patterns of NECAB1/2 were nonoverlapping in the lumbar spinal cord (Fig. 2 *A* and *O*), in contrast to their overlapping expression in DRG neurons.

Anti-NECAB1 antiserum stained neurons and processes in the superficial layers of the dorsal horn and lateral spinal nucleus, as well as, but much less so, in deep layers (laminae III to V) and in lamina X (Fig. 2*A*). NECAB1$^+$ neurons in the superficial layer showed staining in the cytoplasm and proximal dendrites (Fig. 2*B*). Some neurons were bipolar or multipolar, with processes extending in the longitudinal direction (Fig. 2*C*). Some processes also protruded into the white matter outside of lamina I (Fig. 2*A*).

A distinct neuronal subtype was the NECAB1$^+$ neuron with long processes that embraced the border of the dorsal column. Some of these neurons had bipolar processes directed toward the right and left dorsal horns (Fig. 2 *A*, *D*, and *E*). NECAB1$^+$ neurons in the deep layers of the dorsal horn and lateral spinal nucleus were multipolar (Fig. 2 *A* and *C*). Motor neurons in the ventral horn were colabeled for NECAB1 and CGRP (Fig. 2 *A* and *F*).

The analysis of NECAB1-like immunoreactivity (LI) with the CLARITY method provided further insights by visualizing the NECAB1 system in three dimensions (Fig. 2*G* and Movie S1). Thus, the NECAB1$^+$ cell bodies and processes, "embraced" the dorsal column, forming a horseshoe structure (34) with a palisade-like pattern. The bundles of NECAB1$^+$ structures extended from the dorsal commissural region along the medial surface of the dorsal horn, separated by gaps in the longitudinal direction (Fig. 2*H* and Movies S1 and S2). These processes may represent dendrites. However, no axonal process could be identified unequivocally, possibly because of a limited anterograde transport of NECAB1. This group of NECAB1$^+$ neurons has, to our knowledge, not been described in the spinal cord previously.

The giant multipolar neurons in lamina VIII with long processes extending into lamina VII or VI and into the white matter

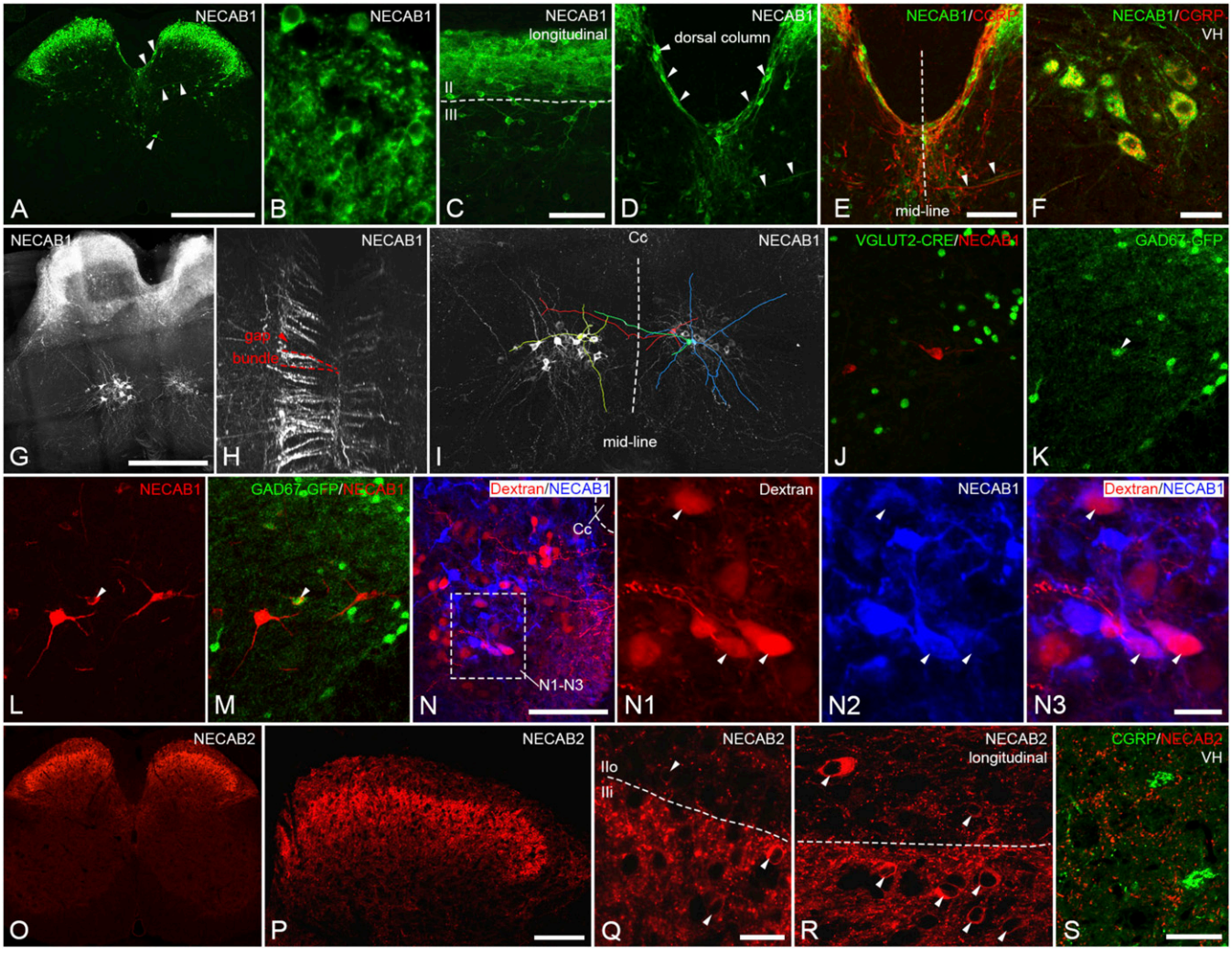

Fig. 2. Expression of NECAB1/2 in lumbar spinal cord. (*A* and *O*) Low-magnification images of NECAB1/2 immunostaining. (*B*) NECAB1-LI in cell bodies and processes in the superficial layers. (*C*) NECAB1$^+$ neurons with different morphologies seen in a sagittal section. (*D* and *E*) NECAB1$^+$ neurons with fibers along the dorsal column. (*F*) NECAB1$^+$ neurons in lamina IX are always CGRP$^+$ (motoneurons). (*G*) NECAB1-LI in spinal cord (CLARITY, 1.0-mm long segment). (*H*) NECAB1$^+$ processes are distributed regularly in bundles along the dorsal column; note that the right side is better stained than the left side (snapshot from NECAB1 CLARITY in Movie S2). (*I*) NECAB1$^+$ neurons in lamina VIII. Green- and red-labeled processes cross the midline (dashed line) whereas blue- and yellow-labeled ones do not (snapshot from Movie S1). Double labeling of NECAB1 with VGLUT2-CRE (*J*) or GAD67-GFP (*K*–*M*) in lamina VIII (arrowhead indicates colocalization). (*N*) Rhodamine red dextran-labeled commissural cells after injection in the contralateral ventral horn (newborn mice). Arrowheads indicate blue-labeled NECAB1$^+$ neurons. (*O*–*R*) NECAB2-LI in cell bodies and boutons in the dorsal horn, mainly laminae IIi and III. (*S*) NECAB2$^+$, CGRP$^-$ boutons in the ventral horn. Arrowheads indicate NECAB2$^+$ neurons in *Q* and *R*. (Scale bars: *A*, *O*, and *G*, 500 μm; *C*, *J*–*N*, and *P*, 100 μm; *D* and *E*, 100 μm; *F* and *S*, 50 μm; *R*, 25 μm; *B*, *Q*, and *N1*–*N3*, 20 μm.)

represent a specific group of cells in the spinal ventral horn (Fig. 2 *A*, *G*, and *I*). They were not excitatory (negative for VGLUT2-driven Cre expression; Fig. 2*J*). A few, however, were inhibitory neurons ($GAD67^{gfp/+}$; indicated by arrowhead in Fig. 2 *K–M*). Retrograde tracing with rhodamine dextran amine showed that the axons of these cells crossed the midline of the spinal ventral horn, and thus represent commissural neurons (Fig. 2*N*). In Fig. 2*I*, some crossing axons have been highlighted with in red and green. Finally, NECAB1$^+$ cells with long processes extending from the lateral spinal dorsal horn (laminae III and IV) joining the midline commissural bundle running between the dorsal column and central canal were observed (Fig. 2 *A*, *D*, and *E*).

NECAB2$^+$ neurons were intensely stained and widely distributed across the spinal cord, extending from lamina IIi to deep layers (laminae III and IV) (Fig. 2 *O* and *P*). Somatic immunoreactivity was often punctate, extending from the cytoplasm into the proximal dendrites, as seen in both the transverse and longitudinal planes (Fig. 2 *Q* and *R* and Fig. 3*E2*). In addition, punctate NECAB2-LI, probably representing boutons, was seen throughout the gray matter, with its highest concentration in the dorsal horn and lamina X (weaker around motor neurons) (Fig. 2 *O* and *P*).

The staining patterns for NECAB1/2 appeared, in general, complementary in the dorsal horn with a narrow band of overlap in lamina IIi (Fig. 3*A*), also seen in longitudinal sections (Fig. 3 *C–E*). Some cases of colocalization in cell bodies were observed in laminae II and III, as well as deep layers (Fig. 3 *A1–B*, and *E1–E3*), and also in the ventral horn close to lamina X (Fig. 3 *C–E*).

NECAB1-LI in the superficial dorsal horn partly overlapped with CGRP$^+$ primary afferents, but no coexistence was seen (Fig. S2 *A* and *B*). NECAB2-LI (laminae IIi to IV) presented a complementary distribution to the CGRP$^+$ plexus (laminae I and IIo) (Fig. S2*E*). Conversely, CGRP-LI could not be detected in the weakly labeled NECAB2$^+$ fibers and varicosities in laminae I and IIo (Fig. S2*F*). With regard to IB4$^+$ boutons, there was some colocalization with NECAB1-LI in midlamina II but not with NECAB2 (Fig. S2 *C*, *D*, *G*, and *H*). In the ventral horn, the puncta were not colocalized with CGRP$^+$ fluorescent dots (Fig. 2*S*).

Colocalization with CaBPs in the Spinal Cord: NECAB1. PV$^+$ neurons are largely restricted to deep lamina II, extending into lamina III (17, 18). A small proportion of NECAB1$^+$ neurons were PV$^+$ in superficial (4.8 ± 1.2%) and deep (15.9 ± 1.9%) layers (Fig. S3 *A* and *B*). Conversely, for PV$^+$ neurons, 31.2 ± 3.7% in superficial layers and 17.3 ± 1.6% in deep layers were NECAB1$^+$. Many CB$^+$ neurons were present in laminae II and III, but only a few were present in deep layers (17). A large population of NECAB1$^+$ neurons in superficial layers coexpressed CB (38.1 ± 2.4%), but less so in deep layers (25.3 ± 3.2%) (Fig. S3 *C* and *D*). For CB$^+$ neurons, 48.5 ± 2.0% in superficial layers and 23.4 ± 2.2% in deep layers were NECAB1$^+$. The percentage of NECAB1$^+$ neurons colocalizing CR in the superficial layers (32.7 ± 3.1%) (Fig. S3 *E* and *F*) was similar to that seen for CB. However, NECAB1-LI colocalized less with CR in deep layers (7.8 ± 0.8%). For CR$^+$ neurons, 44.8 ± 3.1% in superficial layers and 18.0 ± 2.5% in deep layers were NECAB1$^+$. Scgn, with a dense plexus of processes in lamina I and some cell bodies and varicosities in lamina II, did not colocalize with NECAB1-LI (Fig. S3 *G* and *H*).

Colocalization with CaBPs in the Spinal Cord: NECAB2. Because the staining of NECAB2$^+$ cell bodies was not distinct, we did not quantify their colocalization with other CaBPs. Some PV$^+$ neurons, mostly in lamina III, coexpressed NECAB2 (Fig. S3 *I* and *J*). NECAB2$^+$ neurons were frequently CB$^+$ in laminae I–III (Fig. S3 *K* and *L*). Colocalization of NECAB2$^-$ and CR-IR neurons was fairly frequent but mainly restricted to lamina IIi (Fig. S3 *M* and *N*). No colocalization of Scgn and NECAB2-LI was observed (Fig. S3 *O* and *P*).

Phenotyping of NECAB1/2 Dorsal Horn Neurons. To define whether NECAB1/2 label excitatory or inhibitory neurons, we carried out double staining with some established excitatory or inhibitory markers for interneurons in the dorsal horn. PKC-γ is expressed in excitatory interneurons in the deep part of laminae II and III (35). Glutamatergic VGLUT2$^+$ neurons are abundant throughout the spinal cord (3, 36). To identify VGLUT2$^+$ nuclei, we used a BAC-VGLUT2::Cre transgenic mouse line (31) (which

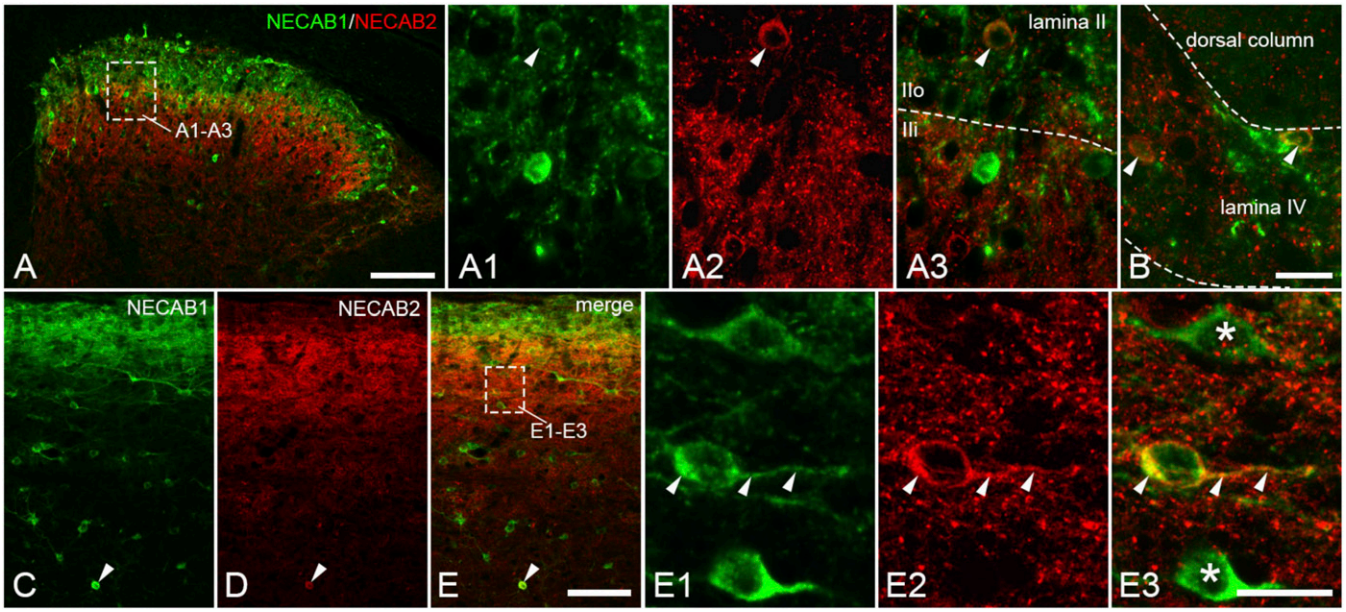

Fig. 3. Complementary distribution of NECAB1/2 in the spinal dorsal horn. (*A* and *B*) NECAB1/2 overlap in lamina IIi. Colocalization of NECAB1$^+$ and NECAB2$^+$ interneurons in laminae II and IV (arrowheads in *A1–A3* and *B*). (*C–E*) Similar expression pattern for the two NECABs in a longitudinal section. Note the distinct morphology of interneurons. NECAB1-LI and NECAB2-LI colocalize in a cell body and process (arrowheads; asterisks label NECAB1-only cells). (Scale bars: *A*, 100 μm; *A1–A3* and *B*, 20 μm; *C–E*, 100 μm; *E1–E3*, 20 μm.)

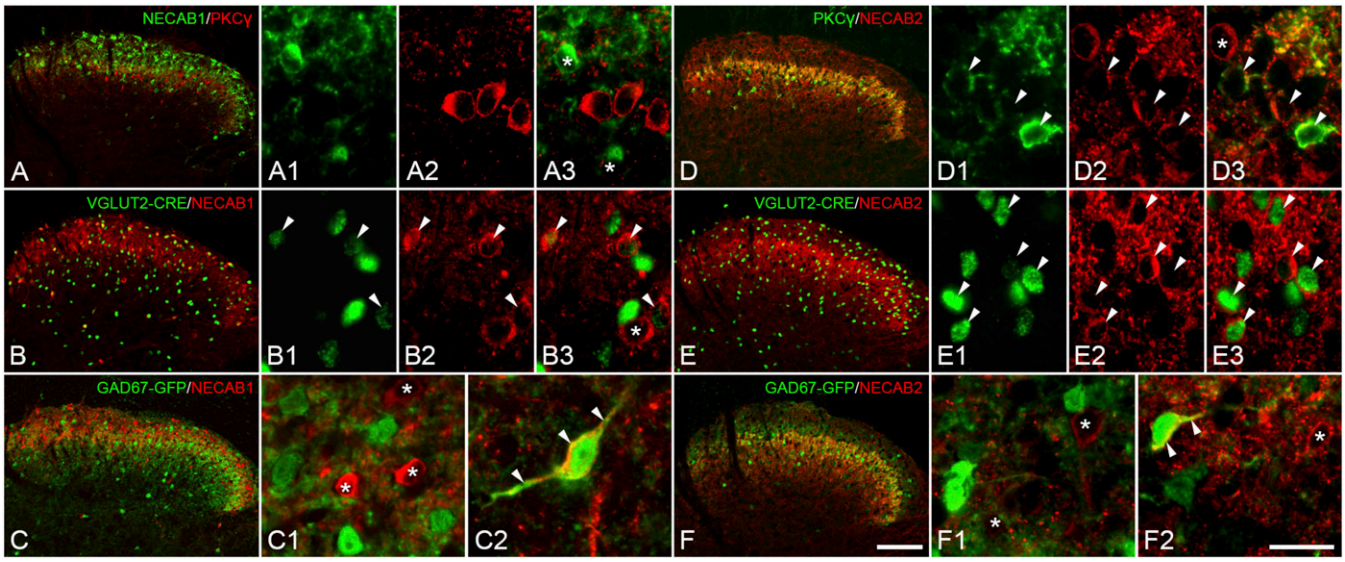

Fig. 4. Coexistence of NECAB1/2 with PKC-γ, VGLUT2, or GAD67 in the spinal dorsal horn. (*A–A3*) NECAB1$^+$ (asterisks) neurons are PKC-γ$^-$. (*B–B3*) NECAB1$^+$ neurons show 70% colocalization with VGLUT2 (arrowheads). (*C–C2*) NECAB1$^+$ neurons usually do not colocalize with GAD67 (asterisks). A few NECAB1$^+$ neurons are GAD67$^+$ in deep layers (arrowheads). (*D–D3*) Most PKC-γ$^+$ neurons in laminae II and III are NECAB2$^+$ (arrowheads). (*E–E3*) Around 90% of NECAB2$^+$ neurons in the spinal dorsal horn are VGLUT2$^+$. (*F–F2*) Single NECAB2$^+$ neurons are GAD67$^+$ (arrowheads). Asterisks indicate NECAB1/2$^+$ neurons that do not colocalize with PKC-γ, VGLUT2, or GAD67. (Scale bars: *A–F*, 100 μm; *A1–A3*, *B1–B3*, *D1–D3*, *E1–E3*, *C1*, *C2*, *F1*, and *F2*, 20 μm.)

reliably captures glutamatergic cells in the spinal cord) in combination with anti-Cre antibodies (37). Similarly, a GAD67$^{gfp/+}$ knock-in mouse line was used to visualize a large subset of inhibitory GABAergic neurons in the spinal cord (32, 38, 39).

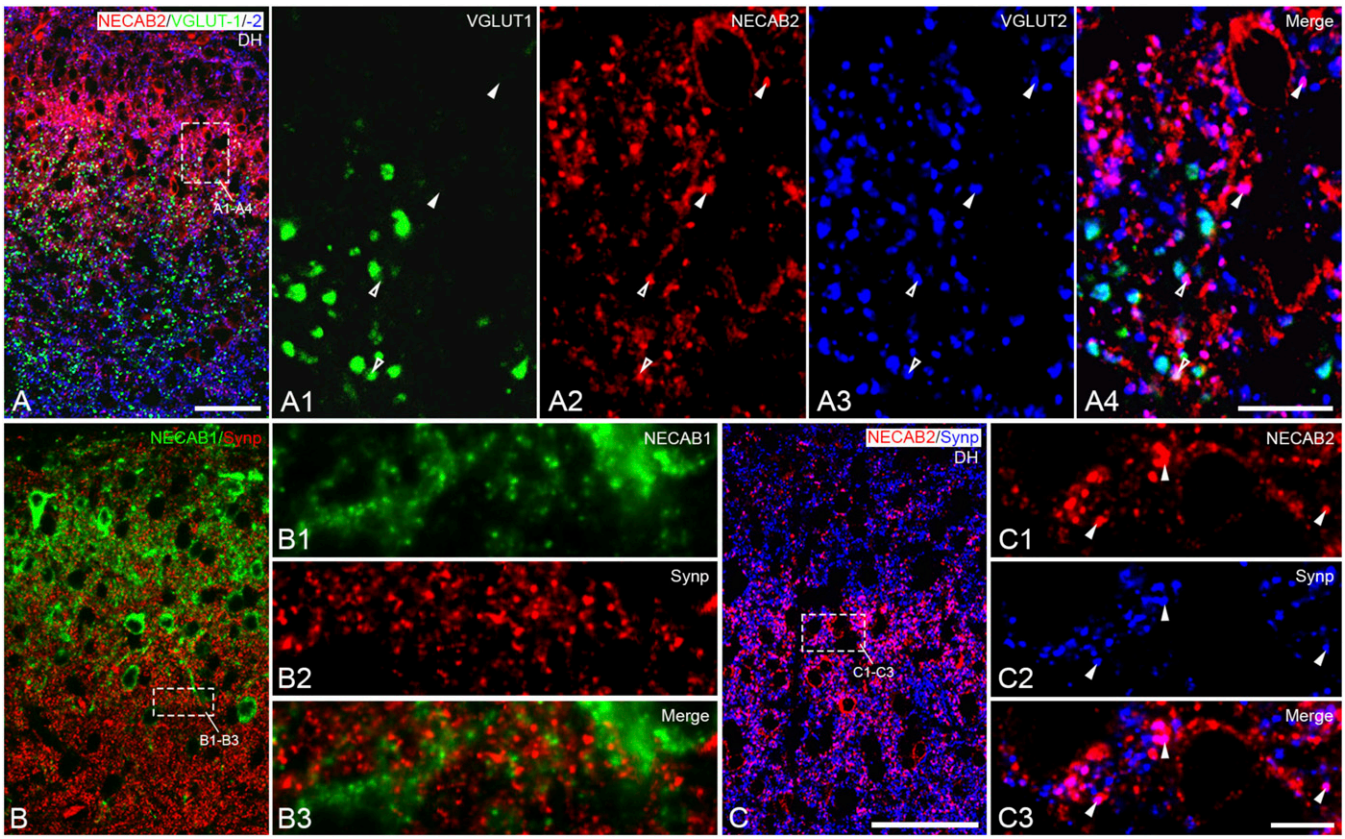

Fig. 5. Coexistence of NECAB1/2 with VGLUT1, VGLUT2, or synaptophysin (Synp) in the spinal cord. (*A–A4*) Most NECAB2$^+$ boutons are VGLUT2$^+$ (solid arrowheads), and some are positive for both VGLUT1 and VGLUT2 (open arrowheads). (*B–B3*) NECAB1 does not colocalize with Synp. (*C–C3*) NECAB2$^+$ boutons are always Synp$^+$. (Scale bars: *A–C*, 50 μm; *A1–A4*, 10 μm; *B1–B3* and *C1–C3*, 5 μm.)

Phenotyping of Dorsal Horn Neurons: NECAB1. These neurons did not stain for PKC-γ, even if there was some regional overlap with this marker in lamina IIi (Fig. 4 *A–A3*). However, the majority of NECAB1$^+$ neurons (72.3 ± 6.9%) in all dorsal horn layers and even in the lateral spinal nucleus were glutamatergic (Cre$^+$; Fig. 4 *B–B3*). Some NECAB1$^+$ neurons in deep layers of the dorsal horn and spinal lateral nucleus colocalized with GAD$^{gfp/+}$, suggesting a GABAergic phenotype (Fig. 4 *C* and *C2*), but only rarely in the superficial layers (Fig. 4*C1*). NECAB1$^+$ neurons were negative for synaptophysin (cf. ref. 40) (Fig. 5 *B–B3*).

Phenotyping Dorsal Horn Neurons: NECAB2. Most of the PKC-γ$^+$ neurons in the spinal dorsal horn were NECAB2$^+$ (Fig. 4 *D–D3*). Furthermore, the majority of NECAB2$^+$ neurons (89.9 ± 0.3%) harbored VGLUT2-driven Cre expression (Fig. 4 *E–E3*). The NECAB2$^+$ neurons lacked GAD67-driven GFP signal (Fig. 4 *F* and *F1*), except for a few cases in deep layers (Fig. 4*F2*). In the dorsal horn, especially in lamina IIi, we found that most NECAB2$^+$ boutons colabeled for VGLUT2, and some of them also colocalized both VGLUT1 and VGLUT2 (Fig. 5 *A–A4*). NECAB2$^+$ boutons were always synaptophysin$^+$ (Fig. 5 *C–C3*).

Axonal Transport of NECABs. The expression of NECAB1-LI and NECAB2-LI in both cell bodies and axons within DRGs raised the question of their centrifugal transport. We found a few NECAB2$^+$ fibers, but no NECAB1$^+$ fibers, in deep dermis of glabrous skin of the hind paw. They were invariably negative for CGRP (Fig. 6*A*). In control sciatic nerve, both NECAB1-LI and NECAB2-LI were frequently observed together with CGRP in, apparently, the same axon, although probably not in the same subcellular compartment (Fig. 6*B*). Sciatic nerve ligation showed accumulation of both NECAB1-LI and NECAB2-LI proximal to the ligation with only weak staining distally, paralleling CGRP (Fig. 6*C*). We also observed NECAB1$^+$ and NECAB2$^+$ axons in the dorsal roots (Fig. 6*D*). As in the sciatic nerve, some NECAB1$^+$ and NECAB2$^+$ axons colocalized with CGRP-LI, but they had a distinctly different subcellular localization (Fig. 6*D*, *Inset*). Taken together, both NECABs are centrifugally transported but their levels in peripheral skin are very low and mostly undetectable with our technique (as discussed above in the section on NECABs in the spinal cord).

Effects of Nerve Injury on NECABs. The results of mRNA expression analysis by qPCR on the effects of axotomy on NECAB1/2 mRNA levels in DRGs and the spinal cord are presented in Fig. 7*A*. Relative NECAB1 mRNA levels in DRGs were not affected 3 d or 2 wk after axotomy. A transient increase in NECAB1 mRNA (1.04 ± 0.12 vs. 1.30 ± 0.13, unscaled expression data; $P = 0.011$) was seen in the ipsilateral spinal cord 3 d after axotomy. Relative NECAB2 mRNA levels were reduced by 50% in DRGs 3 d after denervation, which lasted for up to 2 wk. NECAB2 mRNA levels were not affected in the ipsilateral spinal cord at 3 d. In contrast, a significant elevation was seen after 2 wk (0.99 ± 0.15 vs. 1.34 ± 0.29, unscaled expression; $P = 0.039$).

The effects of nerve injury on total protein levels of NECABs from Western blotting analyses paralleled the changes observed for their respective mRNA transcripts (Fig. 7*B*). In DRG neurons, there was no effect on NECAB1, whereas there was a 40% decrease in NECAB2 protein expression 3 d after axotomy and a 50% decrease 2 wk after axotomy. In the spinal cord, NECAB1 was significantly reduced by 20% after 2 wk (1.00 ± 0.11 vs. 0.79 ± 0.05 arbitrary units of integrated optical density; $P = 0.041$). The expression of NECAB2 in the spinal cord was not affected by injury.

The immunohistochemical analysis of DRGs after nerve injury confirmed the results obtained by biochemistry. The percentage of NECAB1$^+$ NP neurons was modestly but significantly and transiently reduced after 3 d (from 68.1 ± 1.2% to 60.1 ± 2.2%; Fig. 7*C*), with NECAB1 immunofluorescence intensity showing a similar change (Fig. S4). The percentage of small NECAB1 NPs had decreased and the large ones had increased 3 d after injury (Fig. S4). The percentage of NECAB2$^+$ NP neurons significantly decreased to 60% after 3 d and to 40% after 2 wk (Fig. 7*C*), but a reduction in the intensity of NECAB2-LI was only seen 3 d after axotomy (Fig. S4). There was a proportional increase for large NECAB2 NPs 3 d after injury ($P < 0.05$; Fig. S4).

Discussion

The main findings of this study are as follows:

i) NECAB1/2 are expressed in large numbers of lumbar mouse DRG neurons; they coexist with other CaBPs (PV, CB, CR, and Scgn) only to a limited extent and identify a promiscuous Ca^{2+}-binding protein marker for pain-related DRG neurons.

ii) NECAB1/2 are centrifugally transported in DRG neurons, both peripherally and centrally, but their levels in peripheral nerve terminals are low, if not undetectable. This is in strong contrast to the situation for, for example, CGRP (41).

iii) NECAB2 expression in DRGs is regulated by peripheral nerve injury, as is NECAB1/2 expression in the dorsal horn.

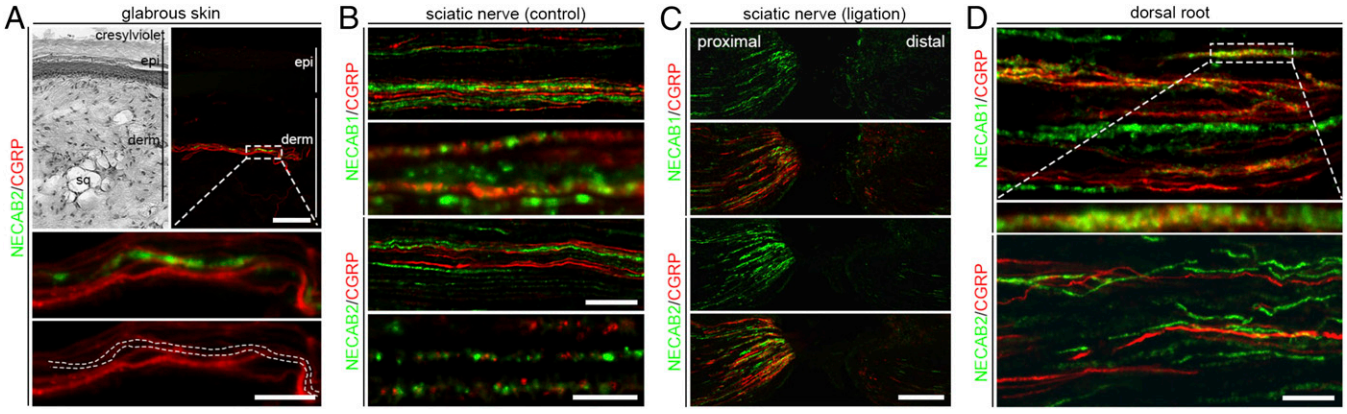

Fig. 6. Presence/transport of NECAB1/2 in DRG axons. (*A*) Only a few NECAB2$^+$, CGRP$^-$ fibers are observed in the dermis of glabrous skin. derm, dermis; epi, epidermis; sq, subcutaneous fat. (*B*) Both NECAB1-LI and NECAB2-LI are observed in the same axon as CGRP but with a different subcellular distribution in control sciatic nerve. (*C*) Both NECAB1-LI and NECAB2-LI accumulate proximal to the sciatic nerve ligation, paralleling CGRP. (*D*) Many NECAB1-IR and NECAB2-IR fibers are observed in the dorsal root. CGRP-LI is seen in a large proportion of NECAB1$^+$ axons but in fewer NECAB2$^+$ axons. [Scale bars: *A*, 50 μm; *Inset* in *A*, 10 μm; *B*, 50 μm (low magnification) and 10 μm (high magnification); *C*, 200 μm; *D*, 20 μm.]

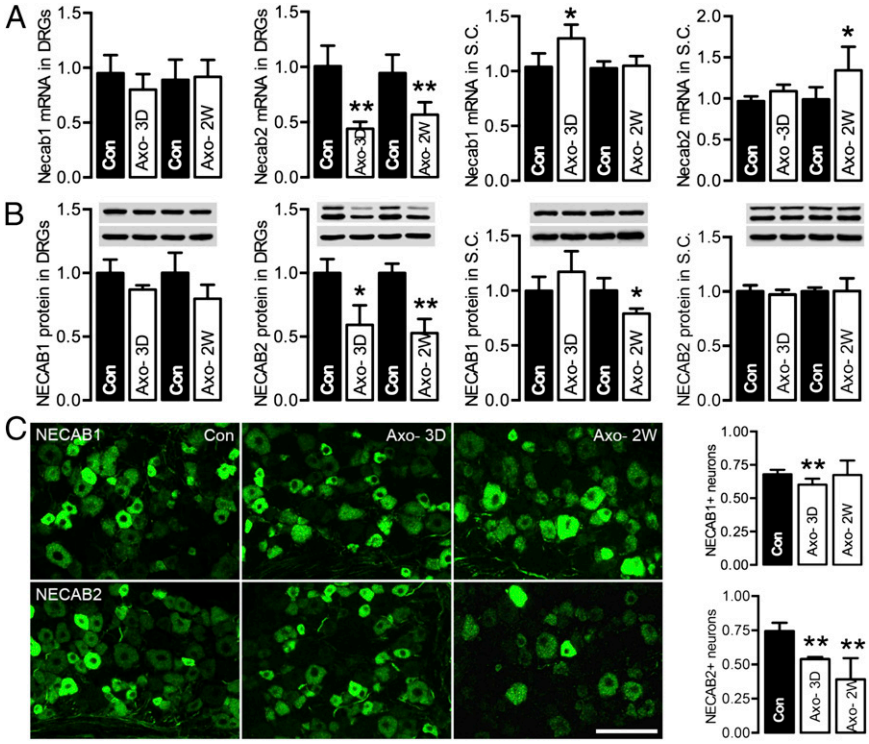

Fig. 7. Effect of peripheral nerve injury on NECABs in DRGs and spinal cord (S.C.). (*A*) Necab1 and Necab2 transcripts (qPCR). The mRNA of Necab1 is only up-regulated transiently in spinal cord (3 d after axotomy). Necab2 is down-regulated in DRGs both 3 d and 2 wk after axotomy, and it is increased in spinal cord 2 wk after axotomy. (*B*) NECAB1/2 proteins (Western blots). The total NECAB1 protein level is reduced in spinal cord 2 wk after axotomy, whereas NECAB2 is down-regulated 3 d and 2 wk after axotomy, but only in DRGs. (*C*) NECAB1/2 in DRG (immunohistochemistry), including quantification (percentage of NPs). The percentage of NECAB1$^+$ NPs is decreased 3 d after axotomy, whereas the reduction of NECAB2 lasts for at least 2 wk. Axo, axotomy; Con, control; 3D, 3 days; 2W, 2 weeks. $*P < 0.05$, $**P < 0.01$. (Scale bar: 100 μm.)

iv) NECAB1/2 are expressed in interneurons in the dorsal horn in a complementary fashion, sometimes colocalized with CB or CR.

v) NECAB1 is expressed in an apparently unique population of neurons that are close to the dorsal column and extend processes in a regular and bundled fashion from the dorsal commissural region along the medial surface of the dorsal horn, possibly connecting the left and right dorsal horns.

vi) NECAB1 identifies a subgroup of commissural neurons in lamina VII.

vii) NECAB$^+$ dorsal horn neurons, especially the NECAB2 positive ones, are mainly glutamatergic.

viii) NECAB2, in contrast to other CaBPs, is not confined to cell bodies/dendrites in the spinal cord but is also present in boutons/nerve endings, suggesting functions innate to synaptic neurotransmission.

ix) NECAB1-LI and NECAB2-LIs were only detected in the cytoplasm, excluding the nucleus, whereas, for example, CB has a strong nuclear staining (17, 33).

Taken together these results suggest that NECAB1/2 may play important but different roles in sensory signaling at the spinal level. In fact, our findings suggest that NECAB1/2 might represent unique CaBPs central to the cellular modulation of mechanosensation, especially pain signaling, at the spinal level.

NECABs in DRGs. NECAB1/2 are both expressed in ∼70% of all DRG neurons, mainly in small- and medium-sized neurons. Thus, they likely exhibit a certain degree of coexistence. They are similarly distributed across all three main categories (42), peptidergic, nonpeptidergic, and myelinated groups of sensory neurons, although NECAB1 is more frequently seen in the nonpeptidergic population.

Fairly little is known about CaBPs in mouse DRG neurons, although Shi et al. (33) showed that 7% are positive for Scgn.

In contrast, more data are available in the rat; however, in this species as well, the expression of classic EF-hand CaBPs (PV, CB, CR, and Scgn) is fairly restricted (18, 33). Thus, ∼14% of DRG neurons are reported to be PV$^+$ and localized in large-diameter neurons (43), with a similar proportion for CB in small-sized neurons (44). Around 10% of medium- to large-sized neurons are CR$^+$ (45), and 3% are Scgn$^+$, exclusively small ones (33). Taken together, in mouse DRGs, the NECAB$^+$ neurons, to date, constitute by far the largest population of CaBP$^+$ neurons. The fact that they represent both peptidergic and nonpeptidergic neurons, with most of them presumably being nociceptors (42), suggests an important role in pain signaling.

NECABs in Spinal Cord: NECAB1. NECAB1-LI is found in bipolar and multipolar neurons in the superficial layers of the dorsal horn and in neurons in deep layers, as well as in motor neurons and multipolar neurons in laminae VII and VIII of the ventral horn.

Spinal dorsal horn neurons represent a highly diverse group of neurons with regard to morphology, neurochemistry, electrophysiological properties, and functions (6, 46–50). Here, we defined the NECAB1$^+$ neurons as mainly excitatory (VGLUT2$^+$, PKCγ$^-$) with only a small proportion being inhibitory (GAD67$^+$), with the latter especially present in the deep layers of the dorsal horn.

Of particular interest are the many NECAB1$^+$ neurons located in the medial aspect of laminae II–IV along the dorsal columns reaching the midline. Most of these cells "climb" on the medial dorsal column wall, but some midline cells can have one process extending into the left dorsal horn and one extending into the right dorsal horn, suggesting that they may convey information between the two sides of the cord. This group of NECAB1$^+$ neurons pos-

sibly labels the dorsal arcuate bundle of dorsal commissural collaterals described by Ramón y Cajal et al. (34). In addition, there are NECAB1$^+$ processes in Ramón y Cajal's middle bundle (34), running together with CGRP fibers. Furthermore, NECAB1$^+$ neurons/processes were also seen associated with one more commissural structures ventral to the central canal (ventral commissural collaterals) (34). Thus, commissural neurons in the medial part of lamina VII were also identified by NECAB1$^+$ expression. These NECAB1$^+$ commissural neurons are embedded in the large group of excitatory and inhibitory commissural neurons located in the ventral spinal cord, which are involved in left/right coordination of locomotion in mice (51–53). The expression of NECAB1$^+$ in a subgroup of commissural neurons may translate into specific functional properties of these groups of cells in coordinating locomotor activity. In summary, NECAB1 is associated with two commissural bundles dorsal to the central canal (dorsal arcuate bundle and middle bundle), as well as with ventral commissural collaterals, which were all described by Ramón y Cajal et al. (34).

NECABs in Spinal Cord: NECAB2. NECAB2 staining is present in neurons with short dendrites in the dorsal horn and, interestingly, in boutons in the gray matter, with the highest density in laminae II–IV and lamina X and a lower density around motoneurons. Punctate staining is also in ventral, lateral, and dorsal columns; however, in longitudinal sections, NECAB2$^+$ descending/ascending axons can be seen. Most of the NECAB2$^+$ neurons/boutons are VGLUT2$^+$ and synaptophysin$^+$. Thus, NECAB2 may play a significant role in controlling Ca^{2+}-dependent processes of exocytosis.

Spinal Cord: NECAB1 vs. CaBPs. With regard to NECAB1, its distribution pattern is quite different from that of PV and Scgn but similar to that seen for CB and CR. The quantification results show that around one-third of the NECAB1-IR neurons are CB$^+$ or CR$^+$ in the spinal dorsal horn, whereas only few NECAB1$^+$ neurons are PV$^+$. In the rat dorsal horn, PV and CB are present in different subclasses of neurons (54, 55). Around 60–70% of the PV$^+$ neurons are GABAergic (laminae II and III), whereas almost all CB$^+$ neurons are excitatory (laminae I–IV) (54). These findings indicate a high degree of complementarity, with around 70% of NECAB1$^+$ neurons being excitatory and those colocalized with PV perhaps being inhibitory.

Spinal Cord: NECAB2 vs. CaBPs. NECAB2, which is sparsely distributed in laminae I and IIo but enriched in laminae IIi and III, shows distinct features compared with CaBPs (essentially rat). Its overall distribution in cell bodies in the dorsal horn is most similar to that of CB. A high proportion of NECAB2$^+$ neurons are also CB$^+$ for boutons in laminae IIi and III. We have already shown here that most of the NECAB2$^+$ neurons are glutamatergic but rarely GABAergic. This is consistent with the established excitatory property of CB$^+$ interneurons in the rat (56). Some NECAB2$^+$ neurons in laminae II and III are colocalized with PV, which labels inhibitory interneurons in rat dorsal horn (6, 54). NECAB2 also shows considerable colocalization with CR$^+$ neurons, mainly in superficial layers, but not with Scgn, which is complementary to the other three classic CaBPs in mouse spinal cord (33).

Taken together, NECAB1/2 neurons are complementary but both still mostly excitatory. Thus, NECAB1/2 neurons probably represent different subgroups of excitatory neurons [i.e., PKC-γ^+ (NECAB2) and PKC-γ^- (NECAB1)], although colocalized in some neurons mainly in lamina IIi.

Axonal Transport of NECABs. NECAB1 (low levels) and NECAB 2 (high levels) can both be seen in normal axons in the sciatic nerve, and they accumulate proximal to a ligation of the nerve (NECAB2 > NECAB1). However, only NECAB2 can be seen in fibers in the paw dermis. We also observed NECAB1$^+$ and NECAB2$^+$ fibers in the dorsal roots, showing that NECABs are also transported centrally. However, NECAB1/2 did not colocalize with CGRP in afferents in the dorsal horn or with IB4, although a limited NACAB1-IB4 coexistence was observed. Overall, these observations suggest that only small amounts of NECAB1/2 reach the peripheral and central nerve endings of the DRG neurons.

Effects of Nerve Injury on NECABs. There was a pronounced down-regulation of NECAB2 in DRG neurons at mRNA and protein levels already 3 d after axotomy and lasting for 2 wk. NECAB1 was not affected significantly, even if partly expressed in the same neurons, showing selectivity. In the spinal cord, the NECAB1/2 transcripts were up-regulated, with the time course of the former preceding that of the latter.

Possible Role of NECABs in Pain Signaling. CaBPs, especially the Ca^{2+} sensors, are important for Ca^{2+}-triggered neurotransmitter release and gene expression in neurons, and they may be important in the neuropathic pain process (7, 13). DREAM (57) is a clearly defined EF-hand Ca^{2+} sensor involved in modulating neuropathic pain as a transcriptional switch for repressing and de-repressing endogenous expression of prodynorphin at the spinal level (central sensitization) (19, 57, 58).

Here, we show a strong effect of nerve injury on the expression of NECAB2 in DRGs and the spinal cord. The function of NECAB2 (Ca^{2+} buffer or sensor) at the spinal level is not known, but studies in some brain regions may give a lead. Thus, in rat hippocampus and hypothalamus, studies on mGluR5 and α2a-adrenergic receptor suggest a sensor role (22, 26). NECAB2 was identified as the interacting protein for the nuclear receptor coactivator vitamin D receptor-interacting protein complex component 150 (59), which also supports a "sensor"-like function for NECAB2 (60). The down-regulation of NECAB2 in the soma of DRG neurons may reduce somatic neurotransmitter release (61) and cross-excitation/cross-depolarization in DRG (62), which are known to contribute to neuropathic pain. If there is a reduction in the afferent nerve endings, synaptic signaling in the dorsal horn could also be attenuated.

It is well established that peripheral nerve injury induces significant changes in the expression of hundreds of molecules in DRG (2, 63, 64). It has been postulated that molecules down-regulated in DRGs after peripheral nerve injury are pronociceptive, a process that serves to protect from pain (11). For example, galanin, which is dramatically up-regulated after nerve injury, has an antinociceptive effect (65), and the pronociceptive excitatory neuropeptides substance P and CGRP are down-regulated (66, 67). The down-regulation of NECAB2 would then indirectly suggest that this CaBP promotes pain signaling by increasing transmitter release from central nociceptive afferents and that its down-regulation aims at counteracting pain. A possible mechanism may be related to mGluR5, which interacts with NECAB2 in rat hippocampal pyramidal cells (26). Thus, previous electron microscopic immunohistochemistry has shown the presence of mGluR5 in primary afferent terminals of rat spinal dorsal horn, and that activation of presynaptic mGluR5 enhances the release of glutamate in the dorsal horn (68, 69). This hypothesis has to be tested in future experiments.

Materials and Methods

Animals. WT male C57BL/6 mice, BAC-Vglut2::Cre mice (31), and GAD67$^{gfp/+}$ reporter knock-in mice (32) were used.

Surgery. Complete transection of the sciatic nerve (axotomy) was performed at the midthigh level, and a 5-mm portion of the distal part was removed to prevent regeneration. Mice were allowed to survive for 3 d or 2 wk. For study of axonal transport, the left sciatic nerve was ligated at the midthigh level and the mice were perfused after 10 h (33).

Labeling of Crossing Spinal Neurons. For anatomical tracing, newborn mice (aged 1–2 d, $n = 4$) were anesthetized with isoflurane before decapitation, and the spinal cords were dissected out in cold 4 °C low Ca^{2+} Ringer's solution containing 111 mM NaCl, 3 mM KCl, 11 mM glucose, 25 mM $NaHCO_3$, 3.7 mM $MgSO_4$, 1.1 mM KH_2PO_4 and 0.25 mM $CaCl_2$, gassed with 95% O_2/5% CO_2 (pH 7.4). After dissection, crossing neurons were labeled retrogradely via application of 3,000-Da rhodamine-labeled dextran amine crystals (Invitrogen/Molecular Probes) paramedial to the midline of the L2 segment, as described previously (39). To allow retrograde labeling of crossing neurons, preparations were incubated for 5–7 h in the dark in oxygenated normal Ringer's solution at room temperature. After incubation, the spinal cords were immersed in 4% (wt/vol) paraformaldehyde for 2 h and processed for immunohistochemistry (39).

Processing of Spinal Cord Tissue for CLARITY. Spinal cords from formaldehyde-acrylamide hydrogel perfused WT adult mice were extracted for CLARITY (30) processing. Incubation in hydrogel monomer solution at 4 °C for 3 d was followed by embedding in polymerized hydrogel by raising the temperature to 37 °C for 3 h. For samples of this size, clarification can be completed by incubation in a solution of 4% (wt/vol) SDS (Amresco) in sodium borate buffer [200 mM (pH 8.5); Sigma] at 37 °C for 4–6 wk, followed by washing for 2 d in PBS + 0.1% Triton X-100 (PBST; Sigma).

To stain intact spinal cords, clarified tissue was incubated in 1% hydrogen peroxide in methanol at 4 °C overnight, followed by washing for 2 d in PBST. Samples were blocked at room temperature overnight using the TSA kit (PerkinElmer), followed by incubation in anti-NECAB1 primary antibody (HPA023629; Atlas Antibodies AB) in PBST (1:100 dilution) at 37 °C for 5 d; they were then washed in PBST at 37 °C for 3 d, incubated in goat anti-rabbit HRP secondary antibody (1:1,000 dilution, PerkinElmer) at 37 °C for 5 d, and washed in PBST at 37 °C for 3 d. Immunoreactivity was visualized with a TSA Cyanine 5 kit (PerkinElmer) following the manufacturer's protocol; samples were then washed in PBST + DAPI (10 ng/mL; Sigma) overnight and placed in FocusClear (CelExplorer) at least 2 h before imaging.

To create 1-mm thick tissue blocks for some of the imaging, samples were embedded in 2% (wt/vol) agarose and cut with a vibratome after clarification. Resulting samples were stained as described above with the following incubation times: hydrogen peroxide (overnight), PBST wash (1 d), blocking (overnight), primary antibody exposure (1 d), PBST wash (1 d), secondary antibody application (1 d), and PBST wash (1 d). Samples were incubated in FocusClear before imaging. The cleared tissue blocks were mounted on coverglass-bottomed dishes (Willco) as previously described (30) and imaged using a water immersion objective with a magnification of 25× and N.A. of 1.05 and a confocal microscope (Olympus). Image stacks were acquired with a z-step spacing of 3 μm or 6 μm. Analysis, volume rendering, and neurite tracings were performed with ImageJ (National Institutes of Health) and Amira software (FEI Visualization Science Group).

Real-Time qPCR. The qPCR reactions were performed with custom-designed primers on a Bio-Rad MyIQ thermal cycler (BioRad Laboratories) (*SI Materials and Methods*).

Immunohistochemistry. For immunohistochemistry, formalin-fixed lumbar (L4 and L5) DRGs, the corresponding lumbar segments of the spinal cord, the sciatic nerve, and the hind leg paws were frozen and sectioned on a cryostat. Sections were processed using the TSA Plus method (PerkinElmer) (*SI Materials and Methods*). Antibodies used in this study were listed in Table S1.

Western Blotting. Total protein samples were separated on 10% SDS/PAGE gels, developed with the enhanced chemiluminescence method, and quantified using Image Lab software (Bio-Rad Laboratories) (*SI Materials and Methods*).

Microscopy and Image Processing. Representative images, and for quantification and analysis of $NECAB^+$ DRG NPs, cross-sectional areas, integrated OD and intensity plots, and colocalization with other markers were acquired on a Zeiss LSM700 confocal laser-scanning microscope. Images were processed using ZEN2012 software (Zeiss). Multipanel figures were assembled using Adobe Photoshop CS6 software (Adobe Systems) (*SI Materials and Methods*). A detailed description of quantification is included in *SI Materials and Methods*.

Statistics. All data were expressed as mean ± SEM and assessed by an unpaired *t* test using Prism 6 software (GraphPad), except for nerve injury data expressed as mean ± SD, which were also analyzed with a *t* test. The criterion for statistical significance was $P < 0.05$.

ACKNOWLEDGMENTS. We thank Profs. Ingrid Nylander (Uppsala University) and Lars Terenius (Karolinska Institutet) for generously supplying the CGRP antiserum, Professor Günter Schütz (German Cancer Center) for the CRE antibody, Professor Takeshi Kaneko (Kyoto University and Japan Science and Technology Corporation) for $GAD67^{gfp/+}$ knock-in mice, Professor Allan Basbaum (University of California, San Francisco) for advice with regard to the size distribution of DRG neurons, and Professor Sandra Ceccatelli (Karolinska Institutet) for valuable advice. Laser-scanning microscopy was made available by the Center for Live Imaging of Cells at Karolinska Institutet Imaging Core facility at the Karolinska Institutet, supported by the Knut and Alice Wallenberg Foundation. Support for this study was provided by the Swedish Medical Research Council (T.H., T.G.M.H., and O.K.); Karolinska Institutet-Delfinansiering (partial financing) of graduate students funds from the Karolinska Institutet (M.-D.Z., T.H., and T.G.M.H.); and funding from the Karolinska Institutet (T.H., T.G.M.H., and O.K.), the Novo Nordisk Foundation (T.H. and T.G.M.H.), the European Research Council (O.K.), the Swedish Brain Foundation (T.H. and T.G.M.H.), the Augusta and Petrus Hedlund Foundation (T.H. and T.G.M.H.), the European Commission's PAINCAGE Seventh Framework Programme integrated project (T.H. and T.G.M.H.), and the Swedish Strategic Foundation (T.G.M.H.).

1. Berridge MJ, Lipp P, Bootman MD (2000) The versatility and universality of calcium signalling. *Nat Rev Mol Cell Biol* 1(1):11–21.
2. Hökfelt T, Zhang X, Wiesenfeld-Hallin Z (1994) Messenger plasticity in primary sensory neurons following axotomy and its functional implications. *Trends Neurosci* 17(1):22–30.
3. Scherrer G, et al. (2010) VGLUT2 expression in primary afferent neurons is essential for normal acute pain and injury-induced heat hypersensitivity. *Proc Natl Acad Sci USA* 107(51):22296–22301.
4. Lagerström MC, et al. (2011) A sensory subpopulation depends on vesicular glutamate transporter 2 for mechanical pain, and together with substance P, inflammatory pain. *Proc Natl Acad Sci USA* 108(14):5789–5794.
5. Rogoz K, Lagerström MC, Dufour S, Kullander K (2012) VGLUT2-dependent glutamatergic transmission in primary afferents is required for intact nociception in both acute and persistent pain modalities. *Pain* 153(7):1525–1536.
6. Todd AJ (2010) Neuronal circuitry for pain processing in the dorsal horn. *Nat Rev Neurosci* 11(12):823–836.
7. Burgoyne RD, O'Callaghan DW, Hasdemir B, Haynes LP, Tepikin AV (2004) Neuronal Ca2+-sensor proteins: Multitalented regulators of neuronal function. *Trends Neurosci* 27(4):203–209.
8. Scholz J, Woolf CJ (2007) The neuropathic pain triad: Neurons, immune cells and glia. *Nat Neurosci* 10(11):1361–1368.
9. Basbaum AI, Bautista DM, Scherrer G, Julius D (2009) Cellular and molecular mechanisms of pain. *Cell* 139(2):267–284.
10. Sandkühler J (2009) Models and mechanisms of hyperalgesia and allodynia. *Physiol Rev* 89(2):707–758.
11. Hökfelt T, Zhang X, Xu X, Wiesenfeld-Hallin Z (2013) Central consequences of peripheral nerve damage. *Textbook of Pain*, eds McMahon S, Koltzenburg M, Tracey I, Turk D (Saunders, Philadelphia), 6th Ed, pp 902–914.
12. Willis WD, Coggeshall RE (2004) *Sensory Mechanisms of the Spinal Cord* (Kluwer/Plenum, New York), 3rd Ed.
13. Mikhaylova M, Hradsky J, Kreutz MR (2011) Between promiscuity and specificity: Novel roles of EF-hand calcium sensors in neuronal Ca2+ signalling. *J Neurochem* 118(5):695–713.
14. Andressen C, Blümcke I, Celio MR (1993) Calcium-binding proteins: Selective markers of nerve cells. *Cell Tissue Res* 271(2):181–208.
15. Klausberger T, Somogyi P (2008) Neuronal diversity and temporal dynamics: The unity of hippocampal circuit operations. *Science* 321(5885):53–57.
16. Freund TF, Buzsáki G (1996) Interneurons of the hippocampus. *Hippocampus* 6(4):347–470.
17. Celio MR (1990) Calbindin D-28k and parvalbumin in the rat nervous system. *Neuroscience* 35(2):375–475.
18. Antal M, Freund TF, Polgár E (1990) Calcium-binding proteins, parvalbumin- and calbindin-D 28k-immunoreactive neurons in the rat spinal cord and dorsal root ganglia: A light and electron microscopic study. *J Comp Neurol* 295(3):467–484.
19. Cheng HY, et al. (2002) DREAM is a critical transcriptional repressor for pain modulation. *Cell* 108(1):31–43.
20. Averill S, Robson LG, Jeromin A, Priestley JV (2004) Neuronal calcium sensor-1 is expressed by dorsal root ganglion cells, is axonally transported to central and peripheral terminals, and is concentrated at nodes. *Neuroscience* 123(2):419–427.
21. Sugita S, Ho A, Südhof TC (2002) NECABs: A family of neuronal Ca(2+)-binding proteins with an unusual domain structure and a restricted expression pattern. *Neuroscience* 112(1):51–63.
22. Canela L, et al. (2007) The neuronal Ca(2+) -binding protein 2 (NECAB2) interacts with the adenosine A(2A) receptor and modulates the cell surface expression and function of the receptor. *Mol Cell Neurosci* 36(1):1–12.
23. Sugita S, Südhof TC (2000) Specificity of Ca2+-dependent protein interactions mediated by the C2A domains of synaptotagmins. *Biochemistry* 39(11):2940–2949.
24. Wolf LV, et al. (2009) Identification of pax6-dependent gene regulatory networks in the mouse lens. *PLoS ONE* 4(1):e4159.

25. Bernier G, Vukovich W, Neidhardt L, Herrmann BG, Gruss P (2001) Isolation and characterization of a downstream target of Pax6 in the mammalian retinal primordium. *Development* 128(20):3987–3994.
26. Canela L, et al. (2009) The association of metabotropic glutamate receptor type 5 with the neuronal Ca2+-binding protein 2 modulates receptor function. *J Neurochem* 111(2):555–567.
27. Lee DS, Tomita S, Kirino Y, Suzuki T (2000) Regulation of X11L-dependent amyloid precursor protein metabolism by XB51, a novel X11L-binding protein. *J Biol Chem* 275(30):23134–23138.
28. Sumioka A, Imoto S, Martins RN, Kirino Y, Suzuki T (2003) XB51 isoforms mediate Alzheimer's beta-amyloid peptide production by X11L (X11-like protein)-dependent and -independent mechanisms. *Biochem J* 374(Pt 1):261–268.
29. Zimmermann B, Girard F, Mészàr Z, Celio MR (2013) Expression of the calcium binding proteins Necab-1,-2 and -3 in the adult mouse hippocampus and dentate gyrus. *Brain Res* 1528:1–7.
30. Chung K, et al. (2013) Structural and molecular interrogation of intact biological systems. *Nature* 497:332–337.
31. Borgius L, Restrepo CE, Leao RN, Saleh N, Kiehn O (2010) A transgenic mouse line for molecular genetic analysis of excitatory glutamatergic neurons. *Mol Cell Neurosci* 45(3):245–257.
32. Tamamaki N, et al. (2003) Green fluorescent protein expression and colocalization with calretinin, parvalbumin, and somatostatin in the GAD67-GFP knock-in mouse. *J Comp Neurol* 467(1):60–79.
33. Shi TJ, et al. (2012) Secretagogin is expressed in sensory CGRP neurons and in spinal cord of mouse and complements other calcium-binding proteins, with a note on rat and human. *Mol Pain* 8:80.
34. Ramón y Cajal S, Azoulay L, Swanson N, Swanson LW (1995) *Histology of the Nervous System of Man and Vertebrates* (Oxford Univ Press, Oxford), Vol 1, pp 265–268.
35. Malmberg AB, Chen C, Tonegawa S, Basbaum AI (1997) Preserved acute pain and reduced neuropathic pain in mice lacking PKCgamma. *Science* 278(5336):279–283.
36. Malet M, et al. (2013) Transcript expression of vesicular glutamate transporters in lumbar dorsal root ganglia and the spinal cord of mice—Effects of peripheral axotomy or hindpaw inflammation. *Neuroscience* 248C:95–111.
37. Kellendonk C, et al. (1999) Inducible site-specific recombination in the brain. *J Mol Biol* 285(1):175–182.
38. Nowak A, et al. (2011) Kv3.1b and Kv3.3 channel subunit expression in murine spinal dorsal horn GABAergic interneurones. *J Chem Neuroanat* 42(1):30–38.
39. Restrepo CE, et al. (2009) Transmitter-phenotypes of commissural interneurons in the lumbar spinal cord of newborn mice. *J Comp Neurol* 517(2):177–192.
40. Melone M, et al. (2004) Localization of the glutamine transporter SNAT1 in rat cerebral cortex and neighboring structures, with a note on its localization in human cortex. *Cereb Cortex* 14(5):562–574.
41. Brumovsky P, Watanabe M, Hökfelt T (2007) Expression of the vesicular glutamate transporters-1 and -2 in adult mouse dorsal root ganglia and spinal cord and their regulation by nerve injury. *Neuroscience* 147(2):469–490.
42. McMahon SB, Priestley JV (2005) *The Neurobiology of Pain* (Oxford Univ Press, Oxford), pp 35–64.
43. Carr PA, Yamamoto T, Karmy G, Baimbridge KG, Nagy JI (1989) Analysis of parvalbumin and calbindin D28k-immunoreactive neurons in dorsal root ganglia of rat in relation to their cytochrome oxidase and carbonic anhydrase content. *Neuroscience* 33(2):363–371.
44. Honda CN (1995) Differential distribution of calbindin-D28k and parvalbumin in somatic and visceral sensory neurons. *Neuroscience* 68(3):883–892.
45. Ren K, Ruda MA, Jacobowitz DM (1993) Immunohistochemical localization of calretinin in the dorsal root ganglion and spinal cord of the rat. *Brain Res Bull* 31(1-2):13–22.
46. Lu Y, Perl ER (2003) A specific inhibitory pathway between substantia gelatinosa neurons receiving direct C-fiber input. *J Neurosci* 23(25):8752–8758.
47. Lu Y, Perl ER (2005) Modular organization of excitatory circuits between neurons of the spinal superficial dorsal horn (laminae I and II). *J Neurosci* 25(15):3900–3907.
48. Hantman AW, van den Pol AN, Perl ER (2004) Morphological and physiological features of a set of spinal substantia gelatinosa neurons defined by green fluorescent protein expression. *J Neurosci* 24(4):836–842.
49. Grudt TJ, Perl ER (2002) Correlations between neuronal morphology and electrophysiological features in the rodent superficial dorsal horn. *J Physiol* 540(Pt 1): 189–207.
50. Dougherty KJ, Sawchuk MA, Hochman S (2005) Properties of mouse spinal lamina I GABAergic interneurons. *J Neurophysiol* 94(5):3221–3227.
51. Kiehn O (2011) Development and functional organization of spinal locomotor circuits. *Curr Opin Neurobiol* 21(1):100–109.
52. Talpalar AE, et al. (2013) Dual-mode operation of neuronal networks involved in left-right alternation. *Nature* 500(7460):85–88.
53. Birinyi A, Viszokay K, Wéber I, Kiehn O, Antal M (2003) Synaptic targets of commissural interneurons in the lumbar spinal cord of neonatal rats. *J Comp Neurol* 461(4): 429–440.
54. Antal M, et al. (1991) Different populations of parvalbumin- and calbindin-D28k-immunoreactive neurons contain GABA and accumulate 3H-D-aspartate in the dorsal horn of the rat spinal cord. *J Comp Neurol* 314(1):114–124.
55. Ren K, Ruda MA (1994) A comparative study of the calcium-binding proteins calbindin-D28K, calretinin, calmodulin and parvalbumin in the rat spinal cord. *Brain Res Brain Res Rev* 19(2):163–179.
56. Albuquerque C, Lee CJ, Jackson AC, MacDermott AB (1999) Subpopulations of GABAergic and non-GABAergic rat dorsal horn neurons express Ca2+-permeable AMPA receptors. *Eur J Neurosci* 11(8):2758–2766.
57. Carrión AM, Link WA, Ledo F, Mellström B, Naranjo JR (1999) DREAM is a Ca2+-regulated transcriptional repressor. *Nature* 398(6722):80–84.
58. Costigan M, Woolf CJ (2002) No DREAM, No pain. Closing the spinal gate. *Cell* 108(3): 297–300.
59. Albers M, et al. (2005) Automated yeast two-hybrid screening for nuclear receptor-interacting proteins. *Mol Cell Proteomics* 4(2):205–213.
60. Alpár A, Attems J, Mulder J, Hökfelt T, Harkany T (2012) The renaissance of Ca2+-binding proteins in the nervous system: Secretagogin takes center stage. *Cell Signal* 24(2):378–387.
61. Huang LY, Neher E (1996) Ca(2+)-dependent exocytosis in the somata of dorsal root ganglion neurons. *Neuron* 17(1):135–145.
62. Amir R, Devor M (1996) Chemically mediated cross-excitation in rat dorsal root ganglia. *J Neurosci* 16(15):4733–4741.
63. Costigan M, et al. (2002) Replicate high-density rat genome oligonucleotide microarrays reveal hundreds of regulated genes in the dorsal root ganglion after peripheral nerve injury. *BMC Neurosci* 3:16.
64. Xiao HS, et al. (2002) Identification of gene expression profile of dorsal root ganglion in the rat peripheral axotomy model of neuropathic pain. *Proc Natl Acad Sci USA* 99(12):8360–8365.
65. Xu XJ, Hökfelt T, Wiesenfeld-Hallin Z (2010) Galanin and spinal pain mechanisms: Past, present, and future. *EXS* 102:39–50.
66. Nielsch U, Bisby MA, Keen P (1987) Effect of cutting or crushing the rat sciatic nerve on synthesis of substance P by isolated L5 dorsal root ganglia. *Neuropeptides* 10(2): 137–145.
67. Noguchi K, Senba E, Morita Y, Sato M, Tohyama M (1990) Alpha-CGRP and beta-CGRP mRNAs are differentially regulated in the rat spinal cord and dorsal root ganglion. *Brain Res Mol Brain Res* 7(4):299–304.
68. Park YK, Galik J, Ryu PD, Randic M (2004) Activation of presynaptic group I metabotropic glutamate receptors enhances glutamate release in the rat spinal cord substantia gelatinosa. *Neurosci Lett* 361(1-3):220–224.
69. Jia H, Rustioni A, Valtschanoff JG (1999) Metabotropic glutamate receptors in superficial laminae of the rat dorsal horn. *J Comp Neurol* 410(4):627–642.

Supporting Information

Zhang et al. 10.1073/pnas.1402318111

SI Materials and Methods

Animals. WT male C57BL/6 mice (adult, 12–14 wk of age) were obtained from SCANBUR AB. BAC- vesicular glutamate transporter 2 (Vglut2)::Cre (1) and glutamate decarboxylase 67 (GAD67)-GFP (2) reporter knock-in mice were also analyzed. The mice were kept under standard conditions on a 12/12-h light/dark cycle with free access to food and water. The experiments were conducted in accordance with Swedish policy for the use of research animals, and were approved by a local ethical committee (Stockholms Norra djurföröksetiska nämnd, N134/12). Efforts were made to minimize the number of mice used and their suffering throughout.

Surgery. Complete transection of the sciatic nerve (axotomy) was performed as described (3). Briefly, mice were anesthetized with 1.7–2.0% (vol/vol) isoflurane (Baxter); the left sciatic nerve was transected at the midthigh level, and a 5-mm portion of the distal part was removed to prevent regeneration. The mice were allowed to survive for 3 d ($n = 30$) or 2 wk ($n = 28$). For study of axonal transport, the left sciatic nerve of mice ($n = 5$) was tightly ligated at the midthigh level with a 6-0 silk suture under anesthesia with isoflurane. The mice were perfused after 10 h.

Tissues. For immunohistochemstry, mice ($n = 15$) and mice undergoing surgery were deeply anesthetized with sodium pentobarbital (50 mg/kg administered i.p.; APL) and perfused transcardially with 4% paraformaldehyde as previously described (4). The lumbar (L4 and L5) dorsal root ganglia (DRGs), the corresponding lumbar segments of the spinal cord, the sciatic nerve, and the hind leg paws were dissected out and postfixed in the same fixative for 90 min at 4 °C, followed by rinsing in 10% (wt/vol) sucrose in 0.16 M phosphate buffer containing 0.01% sodium azide (Merck) and 0.02% bacitracin (Sigma). The tissues were kept in 10% sucrose solution for 2 d at 4 °C. All trimmed tissues were embedded with optimal cutting temperature compound (HistoLab AB), frozen with liquid carbon dioxide, and sectioned on a cryostat (Microm) at a thickness of 12 μm for DRGs, sciatic nerve, and skin, and at 20 μm for spinal cord. The sections were mounted onto glass slides coated with gelatin and stored at −20 °C. For Western blotting and quantitative PCR (qPCR), mice were deeply anesthetized with sodium pentobarbital and decapitated. L4 and L5 DRGs and spinal cord segments were rapidly dissected, frozen on dry ice, and stored at −80 °C until use.

Antibodies. Polyclonal antibodies against neuronal calcium (Ca^{2+})-binding protein 1 (NECAB1) (HPA023629) and NECAB2 (HPA013998) had been generated in the framework of the Human Protein Atlas project (5) and provided by Atlas Antibodies AB. Briefly, rabbits were immunized with human protein epitope signature tags (PrESTs) as antigens (PrEST 135–198 aa for NECAB1 and PrEST 64–198 aa for NECAB2). The two selected PrESTs are highly conserved between *Homo sapiens* and *Mus musculus* (98% identity), making it likely that the antibodies react with mouse NECAB1 or NECAB2. Other antibodies used in this study are listed in Table S1.

Real-Time qPCR. The qPCR reactions were performed with custom-designed primers on a Bio-Rad MyIQ thermal cycler (Bio-Rad Laboratories). Each RNA sample was isolated from DRGs or spinal cord pooled from two mice ($n = 5/N = 10$ for each time point) with the Rneasy Mini Kit (Qiagen). Then, cDNA samples were synthesized using a high-capacity cDNA reverse transcription kit (Applied Biosystems) and amplified with iQ SYBR Green Supermix (BioRad Laboratories). Normalized expression (the difference of threshold cycles between the target gene and house keeping gene, ΔCT) of Necabs was calculated with glyceraldehyde 3-phosphate dehydrogenase (Gapdh) as a housekeeping ("reference") gene (4). Relative mRNA levels were calculated by $2^{-\Delta\Delta CT}$, when the random normalized expression value from the control group was chosen as the calibrator. Each sample was run in triplicate to avoid processing-related deviations (Necab1 forward primer 5′-CCACCTCCAGACGAATTACA-3′, Necab1 reverse primer 5′-CCATGAAGCAGGAACTAGCA-3′, amplicon 100 bp; Necab2 forward primer 5′-CGACAGGACCACTGCAAA-3′, Necab2 reverse primer 5′-CACAGGCAGGCTCTTCATC-3′, amplicon 120 bp).

Immunohistochemistry. Sections were dried at room temperature (RT) for at least 30 min and then incubated with primary antibodies (Table S1) diluted in PBS containing 0.2% (wt/vol) BSA (Sigma) and 0.03% Triton X-100 (Sigma) in a humid chamber at 4 °C for 48 h. Immunoreactivities were visualized using the TSA Plus kit (PerkinElmer) as previously described (4).

For double or triple labeling, we first performed TSA Plus staining and continued with the indirect Coons procedure (6), except in a few cases with double-TSA Plus staining (GFP and NECAB1 in GAD67-GFP mouse spinal cord). After the TSA Plus staining, slides [without 1,4-diazabicyclo[2.2.2]octane (DABCO) mounting] were selected and rinsed in PBS for 10 min and then incubated with primary antibodies over 48 h at 4 °C. The slides were first washed in PBS for 30 min and then incubated with Cy3-conjugated, affinity-purified donkey anti-rabbit (or -mouse, -guinea pig, -goat) IgG (1:150; Jackson Immunoresearch Laboratories) at RT for 90 min; after rinsing, they were mounted in DABCO medium. For triple labeling, the primary antibodies against NECAB2, VGLUT1, and VGLUT2 were mixed together and incubated for 48 h, followed by a mixture of secondary antibodies conjugated with FITC, Cy3, and Cy5. Another set of slides were incubated with isolectin B4 (IB4) from *Griffonia simplicifolia* I (GSA I) (2.5 g/mL; Vector Laboratories), followed by incubation with a goat anti-GSA I antiserum (1:2,000; Vector Laboratories) and incubation with the Cy3-conjugated, affinity-purified donkey anti-goat IgG at RT for 90 min to visualize IB4 binding (7).

Western Blotting. Total proteins were extracted from DRGs and spinal cord by radioimmunoprecipitation assay lysis buffer [50 mM Tris·HCl (pH 7.4), 1% Nonidet P-40, 0.25% sodium deoxycholate, 150 mM NaCl, and 1 mM EDTA] containing protease inhibitor mixture (P8340; Sigma). After sonication, the lysates were centrifuged at 15,300 × *g* for 20 min at 4 °C. The supernatants were collected, and the protein concentrations measured with Bradford Protein Assay (Bio-Rad Laboratories). Laemmli sample buffer (1×, final) containing 20 μg of total protein lysate was loaded in each lane and separated on 10% SDS/PAGE gels, transferred onto PVDF membranes (Millipore), blocked with 5% nonfat dry milk in TBS with 0.1% Tween-20 (TBST) for 1 h at RT, and incubated with antibody against NECABs (anti-rabbit, 1:1,000 in 5% BSA; Atlas Antibodies AB) overnight at 4 °C. The membranes were incubated with HRP-conjugated secondary antibodies for 1 h at RT (1:5,000–1:10,000; DAKO), washed in TBST buffer twice, exposed to ECL solution for 5 min (GE Healthcare), and scanned on a ChemiDOC+ Imaging system (Bio-Rad Laboratories). The membranes were stripped and reprobed with anti-GAPDH antibody (anti-rabbit, 1:1,000 in 5%

BSA; Cell Signaling Technology), used as the loading control. Images were quantified with Image Lab software (Bio-Rad Laboratories) on nonsaturated images.

Microscopy and Image Processing. Representative images were acquired from one airy unit pinhole on an LSM700 confocal laser-scanning microscope (Carl Zeiss) equipped with an objective with a magnification of 5×, an EC Plan-Neofluar objective with a magnification of 10× and N.A. of 0.30, a Plan-Apochromat M27 objective with a magnification of 20× and N.A. of 0.80, and a water objective with a magnification of 40× and N.A. of 1.40. Emission spectra for each dye were limited as follows: FITC (505–540 nm), Cy3 (560–610 nm), and Cy5 (>640 nm). For colocalization analysis of boutons (NECAB2 with synaptophysin, VGLUT1, or VGLUT2), images acquired at an optical thickness of 0.5 μm with an objective with a magnification of 40×. In some cases, orthogonal z-stacks were acquired with a depth interval of 1 μm with an objective with a magnification of 40× (as specified in the figure legends). Images were processed using ZEN2012 software (Zeiss). Multipanel figures were assembled using Adobe Photoshop CS6 software (Adobe Systems).

Quantitative Morphometry. For quantification of neuron profiles (NPs) of NECAB$^+$ DRG neurons, three to five L5 DRG sections, immunostained for NECABs and counterstained with 0.001% propidium iodide (PI; Sigma) (n = 5), were selected from different levels (usually a four-section interval). Sections were tile-scanned with an LSM700 laser-scanning microscope equipped with a Plan-Apochromat M27 objective with a magnification of 20× and N.A. of 0.80. The intensity of NECAB-like immunoreactivity in neurons higher than mean plus two folds of SD of the soma of negative neurons from each section was considered positive. The total number of DRG NPs was counted on PI-stained specimens. All of the counting, including the quantification of colocalization, was performed using Adobe Photoshop CS6 software. The cross-sectional area and intensity (mean gray value) of NECAB$^+$ neurons were also collected using ImageJ v.1.46 software (National Institutes of Health). Only NECAB$^+$ neurons with a clear nucleus were collected, and the background for each ganglion was subtracted for intensity quantification. Size distribution of NECAB$^+$ DRG neurons was performed according to the method of Scherrer et al. (8) using size cutoff classification criteria as follows: small (<300 μm^2), medium (300–700 μm^2), and large (>700 μm^2).

For the quantification of colocalization between NECABs and calcitonin gene-related peptide, IB4, neurofilament 200, or Ca^{2+}-binding proteins (CaBPs) in DRGs, three to five slides (for each marker) of DRG sections (n = 5) were double-stained, tile-scanned (with an objective with a magnification of 20×), and counted using Photoshop CS6. Colocalization between NECAB1 and CaBP$^+$ interneurons in spinal dorsal horn was assessed using the same procedure. We refrained from quantifying NECAB2-CaBP colocalization, because the staining of NECAB2$^+$ cell bodies was not distinct (in contrast to that of NECAB1). We only performed a quantification of NECAB2 with VGLUT2 or GAD67 in the spinal dorsal horn. The assessment of colocalization between NECABs and VGLUT2-CRE or GAD67-GFP$^+$ neurons in spinal dorsal horn was based on two transgenic mice per strain. Before the quantification of colocalization between the cytoplasmic NECAB1 or NECAB2 and nucleus Cre staining, we performed the 3D laser scanning randomly to confirm the naturally complementary colocalization of the cytoplasm and nucleus.

1. Borgius L, Restrepo CE, Leao RN, Saleh N, Kiehn O (2010) A transgenic mouse line for molecular genetic analysis of excitatory glutamatergic neurons. *Mol Cell Neurosci* 45 (3):245–257.
2. Tamamaki N, et al. (2003) Green fluorescent protein expression and colocalization with calretinin, parvalbumin, and somatostatin in the GAD67-GFP knock-in mouse. *J Comp Neurol* 467(1):60–79.
3. Wall PD, et al. (1979) Autotomy following peripheral nerve lesions: Experimental anaesthesia dolorosa. *Pain* 7(2):103–111.
4. Shi TJ, et al. (2012) Secretagogin is expressed in sensory CGRP neurons and in spinal cord of mouse and complements other calcium-binding proteins, with a note on rat and human. *Mol Pain* 8:80.
5. Uhlen M, et al. (2010) Towards a knowledge-based Human Protein Atlas. *Nat Biotechnol* 28(12):1248–1250.
6. Coons AH (1958) Fluorescent antibody methods. *Gen Cytochem Methods* 1:399–422.
7. Wang H, Rivero-Melián C, Robertson B, Grant G (1994) Transganglionic transport and binding of the isolectin B4 from Griffonia simplicifolia I in rat primary sensory neurons. *Neuroscience* 62(2):539–551.
8. Scherrer G, et al. (2010) VGLUT2 expression in primary afferent neurons is essential for normal acute pain and injury-induced heat hypersensitivity. *Proc Natl Acad Sci USA* 107 (51):22296–22301.

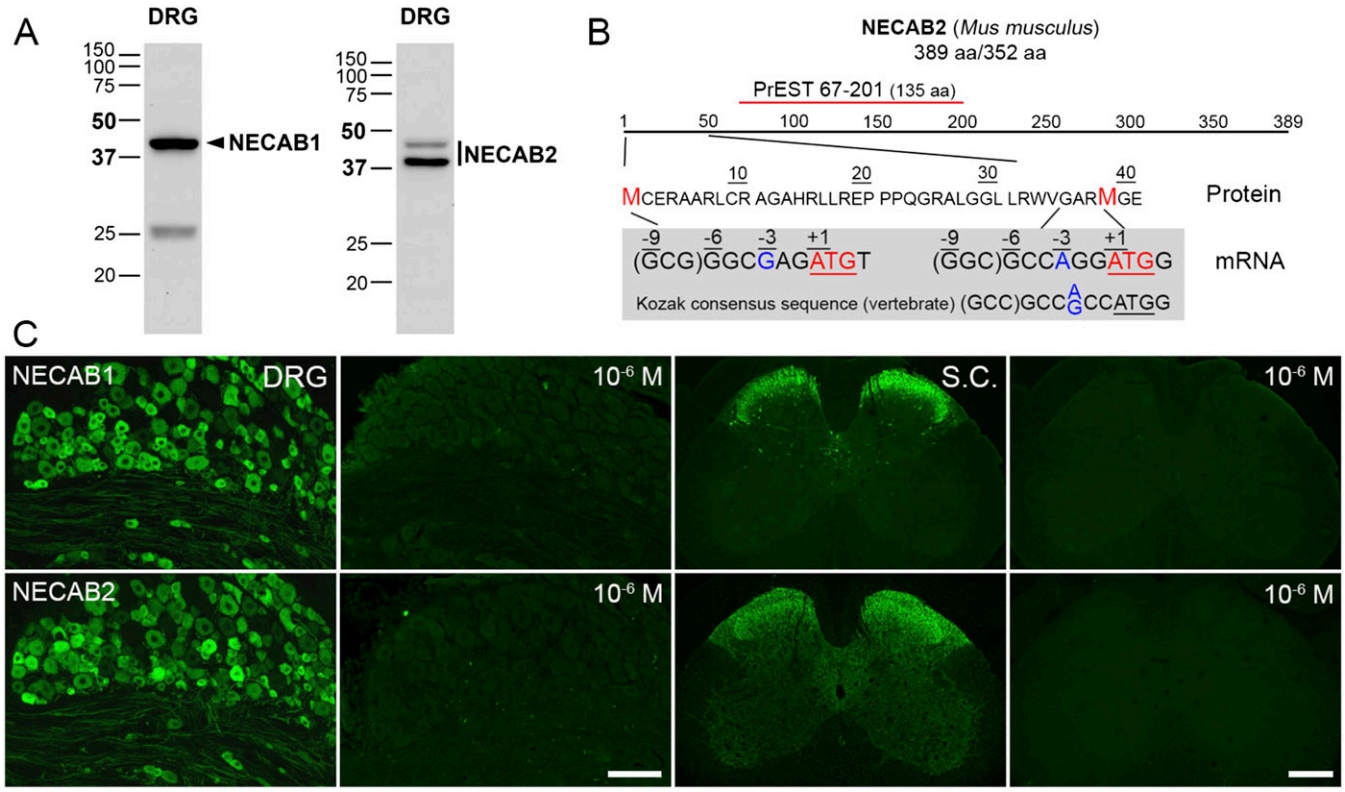

Fig. S1. Characterization of NECAB1/2 antibodies. (*A*) Western blot shows one single band between 37 kDa and 50 kDa specific for NECAB1 and two bands corresponding to two NECAB2 isoforms in DRGs lysates. The specific bands are indicated by an arrowhead and vertical line. (*B*) Immunogen (PrEST) locations for NECAB2 are present in the drawing with red lines below the protein amino acids. There are two Kozak consensus sequences in Necab2 mRNA listed with nucleotide sequences from positions −9 to +4, which produce two NECAB2 isoforms. (*C*) Confocal images of one single optical section show NECAB1/2 present in both lumbar DRGs and the spinal cord (S.C.). The NECAB-like immunoreactivities are depleted in the adjacent sections after adding 10^{-6} M immunogen in the antigen adsorption experiment. (Scale bars: *C*, 100 μm for DRG and 250 μm for spinal cord.)

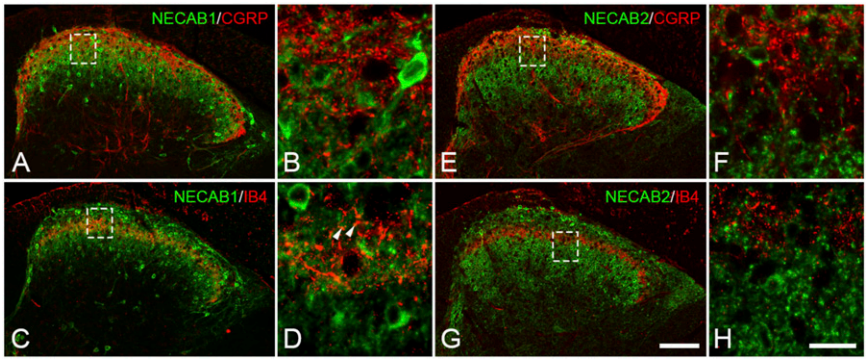

Fig. S2. Double staining of NECABs with calcitonin gene-related peptide (CGRP) or IB4 in the spinal dorsal horn. (*A* and *B*) NECAB1-LI was not colocalized with CGRP. (*C* and *D*) However, some NECAB1^{+} puncta staining was IB4^{+}. (*E* and *F*) No colocalization of NECAB2^{+} boutons with CGRP^{+} puncta was observed. (*G* and *H*) Neither was there any coexistence between NECAB2 and IB4. (Scale bars: *A*, *C*, *E*, and *G*, 100 μm; *B*, *D*, *F*, and *H*, 20 μm.)

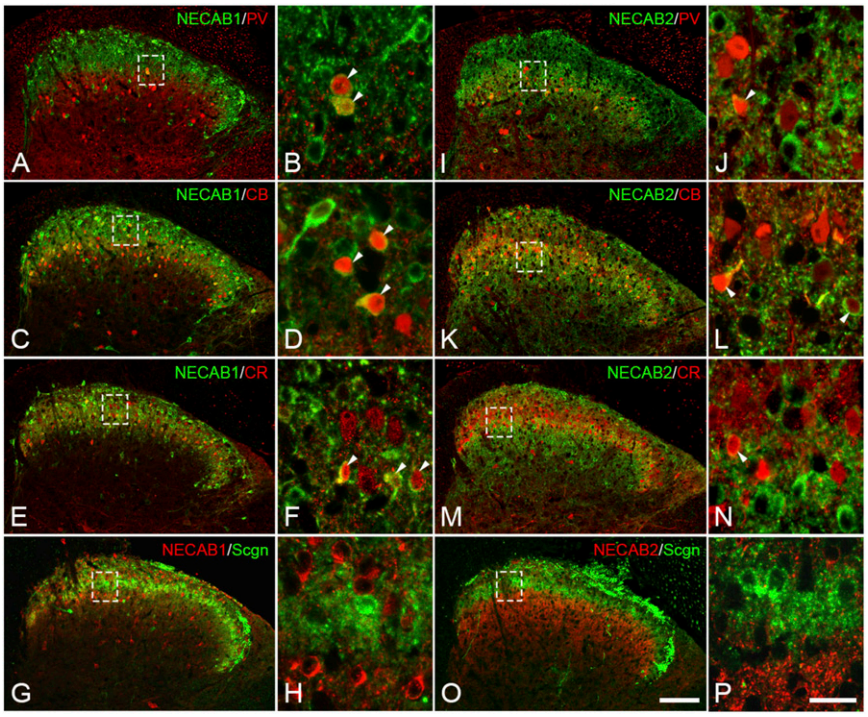

Fig. S3. Double staining of NECABs with CaBPs in spinal dorsal horn. Confocal images show NECABs plus parvalbumin (PV), calbindin D-28K (CB), calretinin (CR), or secretagogin (Scgn) with low (*A*, *C*, *E*, *G*, *I*, *K*, *M*, and *O*) and high magnification (*B*, *D*, *F*, *H*, *J*, *L*, *N*, and *P*). High magnification views are from rectangles in *A*, *C*, *E*, *G*, *I*, *K*, *M*, and *O*, respectively. Arrowheads indicate examples of colocalization of NECABs with CaBPs. Note that NECAB − Scgn colocalization was not detected. (Scale bars: *A*, *C*, *E*, *G*, *I*, *K*, *M*, and *O*, 100 μm; *B*, *D*, *F*, *H*, *J*, *L*, *N*, and *P*, 20 μm.)

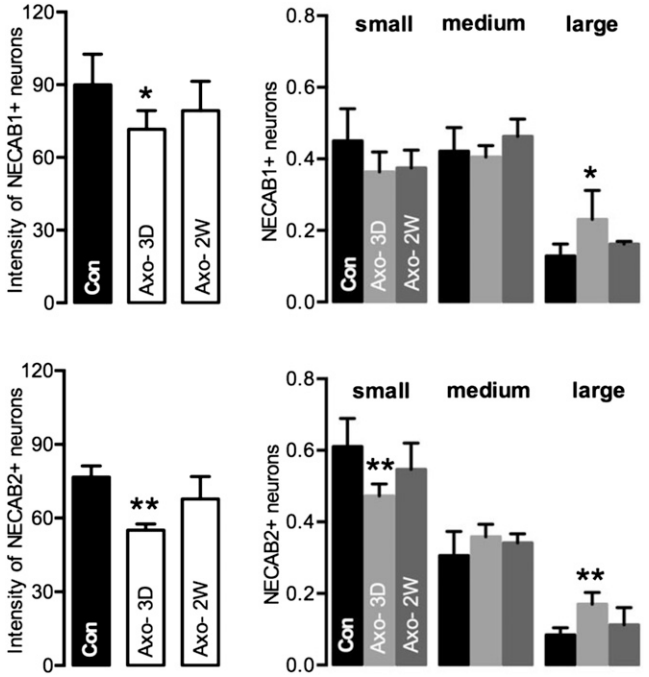

Fig. S4. Effects of nerve injury on intensity and size distribution of NECAB$^+$ neurons (n = 2,503 for NECAB1 and n = 3,885 for NECAB2). Axo, axotomy; Con, control; 3D, 3 days; 2W, 2 weeks. *P < 0.05, **P < 0.01.

Table S1. Primary antibodies used in this study

Antibody	Host	Antigen	Supplier/catalog no.	Dilution
NECAB1	Rabbit polyclonal	Amino acids 39–102 of human NECAB1	Atlas Antibodies AB/HPA023639	1:1,000
NECAB2	Rabbit polyclonal	Amino acids 64–198 of human NECAB2	Atlas Antibodies AB/HPA013998	1:10,000
CGRP	Rabbit polyclonal	Tyr-αr CGRP (23–37) and thyroglobulin	L. Terenius (Karolinska Institutet, Stockholm) and I. Christensson (Uppsala University, Uppsala)	1:20,000
NF200	Mouse monoclonal	C-terminal segment of enzymatically dephosphorylated pig NF200	Sigma/N0142	1:400
Parvalbumin	Rabbit polyclonal	Rat muscle parvalbumin	Swant/PV 25	1:400
Calbindin D-28K	Rabbit polyclonal	Rat recombinant calbindin D-28K	Swant/CB 38	1:400
Calretinin	Rabbit polyclonal	Human recombinant calretinin	Swant/7699/3H	1:400
Secretagogin	Rabbit polyclonal	Amino acids 135–273 of human secretagogin	Atlas Antibodies AB/HPA006641	1:400
VGLUT1	Goat polyclonal	C-terminal sequence of mouse VGLUT1 (amino acids 531–560)	M.W.	1:300
VGLUT2	Guinea pig polyclonal	C-terminal sequence of mouse VGLUT2 (amino acids 549–582)	M.W.	1:500
Synaptophysin	Mouse monoclonal	Pentapeptide repeat structure in the C-terminus of synaptophysin	Millipore/MAB5258	1:1,000
GFP	Chicken polyclonal	Recombinant full-length GFP	Abcam/ab13970	1:4,000
PKC-γ	Rabbit polyclonal	C terminus of mouse PKC-γ	Santa Cruz Biotechnology/sc-211	1:2,000
Cre	Rabbit polyclonal	Recombinant protein nucleus localization signal and Cre	G. Schütz (German Cancer Center, Heidelberg, Germany)	1:4,000

CGRP, calcitonin gene-related peptide; NF200, neurofilament 200.

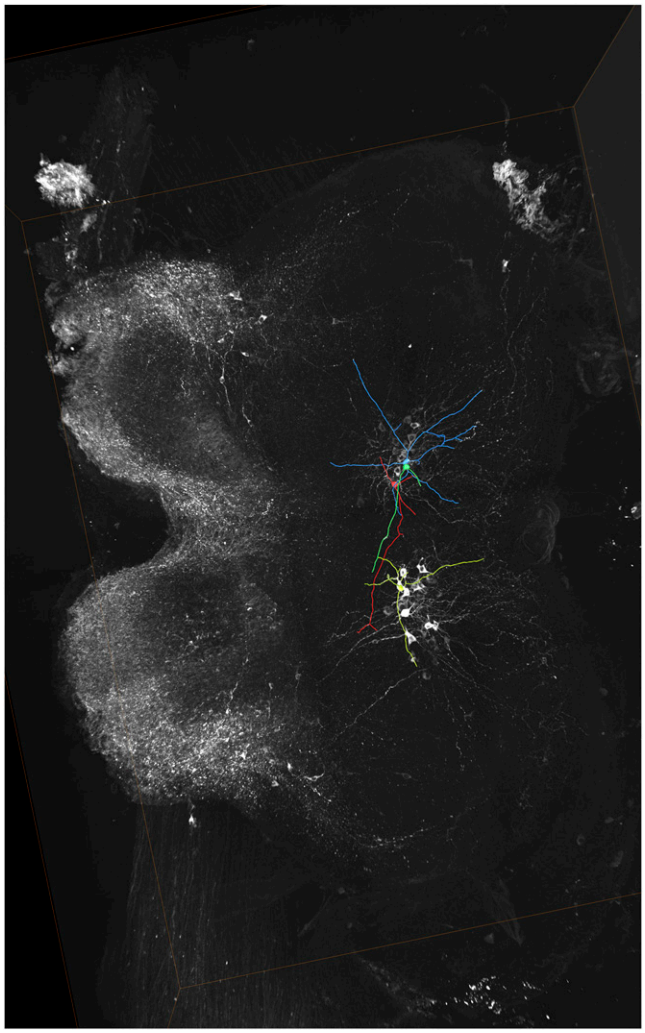

Movie S1. The movie shows a series of NECAB1^{+} images through the 3D reconstruction data from mouse lumbar spinal cord (1-mm thickness) after the CLARITY process.

Movie S1

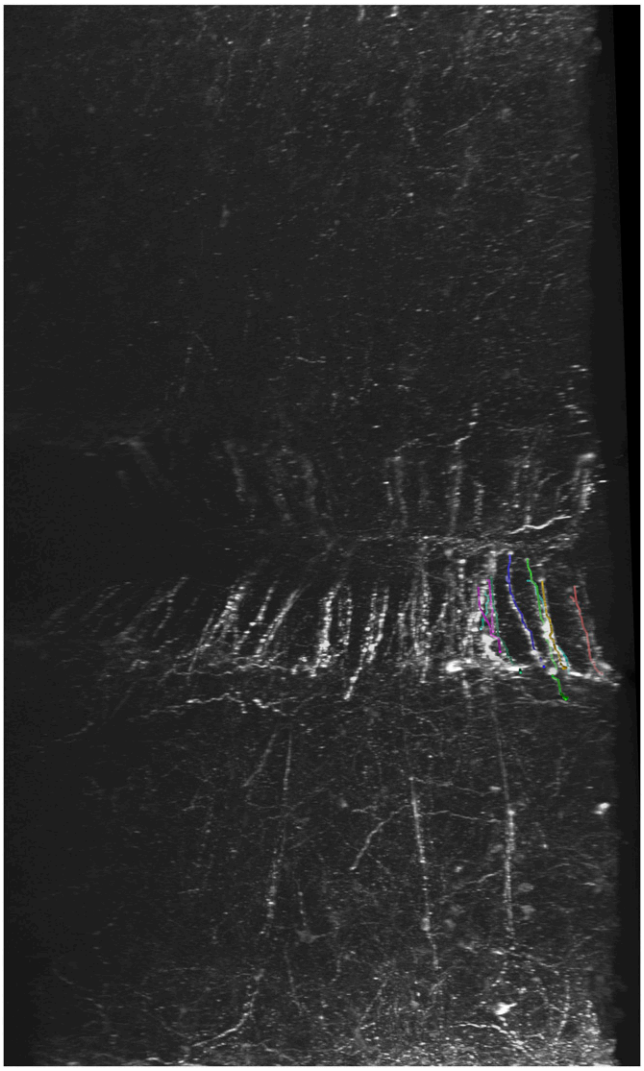

Movie S2. The movie shows a series of NECAB1^{+} images through the 3D reconstruction data from mouse lumbar spinal cord with the emphasis on the NECAB1^{+} bundles along the dorsal column.

Movie S2